Evaluating estuarine sediment provenance from geochemical patterns in upper Chesapeake Bay

Emily Russ*, Cindy Palinkas, Jeff Cornwell

Horn Point Laboratory, University of Maryland Center for Environmental Science

Cambridge, MD 21613, USA

*Corresponding Author

E-mail address: eruss@umces.edu

Abstract

Geochemical patterns in upper Chesapeake Bay sediments can reflect a variety of important processes. Spatial and down-core geochemical patterns are useful for understanding the underlying conservative (sediment provenance) and non-conservative (salinity, redox, anthropogenic influences) processes driving these patterns. Distinguishing conservative and non-conservative processes to quantify sediment sources will help develop management strategies to limit excess sedimentation in estuaries. In this study, elemental concentrations were measured via inductively coupled plasma mass spectroscopy (ICP-MS) and analyzed using principal component analysis. The sediment geochemistry data were then analyzed to evaluate contributions of Susquehanna River and shoreline erosion to bottom sediments in the upper Bay using a sediment-provenance analysis. Elements associated with aluminosilicate minerals, which were sensitive to grain-size changes, and rare earth elements, which were sensitive to salinity changes, explained the most variability in the dataset. Variability in heavy metal concentrations demonstrated decadal changes in anthropogenic inputs. The results from the sediment-provenance analysis indicated that the Susquehanna River is the dominant source of fine sediment in the upper Bay.

1. Introduction

Spatial patterns of geochemical signatures in estuarine sediments reflect a variety of important processes, depending on element behavior. For example, conservative geochemical tracers, such as Al, Li, and ratios of rare earth elements (REEs), reflect sediment provenance (Loring 1991; Windom et al. 1989; Munksgaard et al. 2003), while non-conservative tracers, such as organic matter, Fe and Mn, total REE concentrations, and heavy metals reveal changes in

salinity, redox conditions, and/or anthropogenic influences (Sholkovitz and Elderfield 1988; Bricker 1993; Owens and Cornwell 1995; Guo et al. 1997; Zimmerman and Canuel 2000; Spencer et al. 2003). Elements can also behave differently depending on environmental context, such as Fe and P, which are relatively conservative in fresh water under oxidizing conditions but non-conservative in salt water under hypoxic conditions (Guo et al. 1997; Jordan et al. 2008). For sediment provenance, it is important to analyze as many parameters as possible and interpret them within a specific environmental context.

Historically, analytical constraints have limited the number of samples and/or elements considered by individual studies, hindering interpretation of the geochemical record preserved in sediment cores. For example, most previous studies have been restricted to a specific group of elements (i.e. trace elements, heavy metals, or rare earth elements) and have limited scope, focusing on either spatial patterns of surface sediments or down-core changes at individual sites (e.g. previous work in Chesapeake Bay by Sinex and Helz 1981; Sholkovitz and Elderfield 1988; Owens and Cornwell 1995; Zimmerman and Canuel 2000). Recent advancements in analytical techniques, particularly inductively coupled plasma mass spectroscopy (ICP-MS), now allow analysis of >50 elements on small amounts of sediment for a relatively low cost, greatly expanding datasets needed for robust understanding of geochemical patterns in space and time.

These datasets often have high dimensionality and contain co-varying elements, making statistical analyses challenging; however, techniques such as correlation and principal component analyses reduce dimensionality and highlight underlying relationships in the data (Reid and Spencer 2009; Hannigan et al. 2010; Prajith et al. 2016). These advances allow the competing influences of conservative (sediment provenance) and non-conservative (salinity, redox, anthropogenic influence) processes on sediment geochemistry to be untangled, which is

54 critical for using these data to address many scientific and management issues. For example,
55 reducing fine sediment input is a major management focus in coastal and estuarine areas, as
56 excess fine sediment is one of the main pollutants degrading water quality (Thrush et al. 2004;
57 US EPA 2010; USACE 2015). Conversely, sediment can also be an important resource for
58 maintaining and sustaining wetland habitats that are threatened by sea-level rise (e.g. Blum and
59 Roberts 2009; Kirwan and Megonigal 2013). However, the former is the focus of this study.
60 Sediment-provenance analyses, which quantify sediment contributions from distinct sources,
61 provide the data needed to develop effective sediment-management strategies (Mukundan et al.
62 2012). Sediment-provenance analyses employ a suite of geochemical parameters (i.e. trace
63 metals, nutrients, radioisotopes, and stable isotopes) to produce a characteristic signature for
64 individual sediment sources. These signatures can then be used to quantify the relative
65 contributions of source materials to suspended or bottom sediments. For example, sediment-
66 provenance analyses have been used to quantify source contributions from surface and
67 subsurface sediments in rivers (Walling 2005) and deltaic floodplains (Jalowska et al. 2017), and
68 to determine contributions of different land uses (Gellis and Noe 2013; Voli et al. 2013) and
69 physiographic provinces (Devereux et al. 2010) to suspended-sediment loads.
70 Understanding the fate of sediment sources in the Chesapeake Bay is critical for
71 developing targeted sediment-management approaches, especially with respect to recent total
72 maximum daily load (TMDL) sediment reduction goals (US EPA 2010). Sediment-provenance
73 analyses can potentially differentiate between sediments delivered from the Bay's main tributary,
74 the Susquehanna River, and those eroded from shorelines, but these analyses require
75 conservative element differentiation. There is limited information from previous studies on the
76 geochemical character of sediments from the Susquehanna River, shoreline sediments, and upper

77 Bay. Thus, the first step in determining provenance of Bay sediments is to identify the most
78 prevalent elements and whether they are conservative or non-conservative in the estuary. This
79 study takes advantage of relatively new analytical and statistical analyses of sediment
80 geochemistry to take this first step and move forward to applying the results to a sediment-
81 provenance analysis, providing a foundation for future work. Specifically, the objectives are to:
82 1) identify the most prevalent conservative and non-conservative elements in upper Bay
83 sediments; 2) describe spatial patterns in surficial sediments and with depth in cores; 3)
84 determine the underlying processes driving the observed patterns; and 4) evaluate the potential
85 for results to quantify relative contributions of Susquehanna River and shoreline sediments to
86 upper Bay sediments.
87
88 **2. Methods**
89 *2.1 Study Site*
90 The upper Chesapeake Bay is the ~100 km section between the Susquehanna River and
91 Choptank River mouths (Fig. 1A). Here, the Bay varies in width between 5 km and 20 km.
92 Although the narrow main stem Bay channel reaches depths up to 53 m south of Annapolis, the
93 average depth of this portion of the Bay is only 4 m due to broad shallow shoals flanking the
94 main channel (https://www.ngdc.noaa.gov/mgg/bathymetry/estuarine/). The tidal range is lowest
95 near Annapolis at 0.3 m, increases to 0.4 m near Baltimore, and further increases to 0.6 m at the
96 head of the Bay. Tidal currents are also lowest near Annapolis at 0.13 m s^{-1}, increase to 0.6 m s^{-1}
97 near Baltimore, then decrease north of Baltimore to 0.2 m s^{-1} at the head of the Bay (Zhong and
98 Li 2006). Significant wave heights in the upper Bay are typically <1 m with a mean period <2.5 s

99 (https://buoybay.noaa.gov/). These waves are generally fetch-limited and generated by winds
100 (Sanford 1994).

101 There are three salinity regions in the upper Bay: tidal freshwater (0-0.5), from the
102 Susquehanna River mouth to Turkey Point; oligohaline (0.5-5), from Turkey Point to the
103 Patapsco River mouth; and mesohaline (5-18), from the Patapsco River mouth to the Potomac
104 River estuary mouth (http://eyesonthebay.dnr.maryland.gov/). These salinity regions are largely
105 influenced by freshwater discharge from the Susquehanna River, which delivers >80% of the
106 total freshwater to the upper Bay (Schubel and Pritchard 1986). River discharge is generally
107 highest during the spring, pushing the saltwater front farther seaward, and lowest during the
108 summer, allowing the saltwater front to migrate farther landward (Schubel and Pritchard 1986).

109 The Susquehanna River is also the primary source of sediment to the upper Bay,
110 supplying ~$2x10^6$ t annually (Langland 2015). Much of this sediment is trapped northward of
111 39°10' N (~40 km from the Susquehanna River mouth) in the estuarine turbidity maximum
112 (ETM) (Biggs 1970; Schubel and Pritchard 1986; Donoghue et al. 1989). Shoreline erosion is
113 another significant source of sediment to the upper Bay, contributing ~$1.0x10^6$ t y^{-1}, and
114 becoming the dominant source south of the ETM (Schubel 1968; Biggs 1970; calculated after
115 applying dry bulk density correction factor from Langland and Cronin (2003)). This value
116 reflects fastland erosion (erosion above mean high water (MHW), and was used interchangeably
117 with shoreline erosion in this study) but not nearshore erosion, which can more than double this
118 value when included (Langland and Cronin 2003). Sediment grain sizes in the upper Bay range
119 from sandy-silts to silty-clays, although shorelines are predominately sandy (Kerhin 1988; Hobbs
120 et al. 1994).

Previous research of sediment geochemistry in the upper Bay focused on surficial sediments, showing that several elements (Mn, Fe, Co, Ni, and Cu) decrease with distance from the Susquehanna River and that heavy metals (Zn, Cd, and Pb) are enriched due to anthropogenic influences (Sinex and Helz 1981). Also, analysis of particulate Fe suggested that the Susquehanna River contributes 85% of the material in the upper Bay, with shoreline erosion supplying 15% (Helz et al. 1985). Lastly, while dissolved concentrations of rare earth elements (La, Ce, Pr, Nd, Sm, Eu, Gd, Dy, Y, Er, Yb) were studied, few reports of sediment concentrations exist (Sholkovitz and Elderfield 1988).

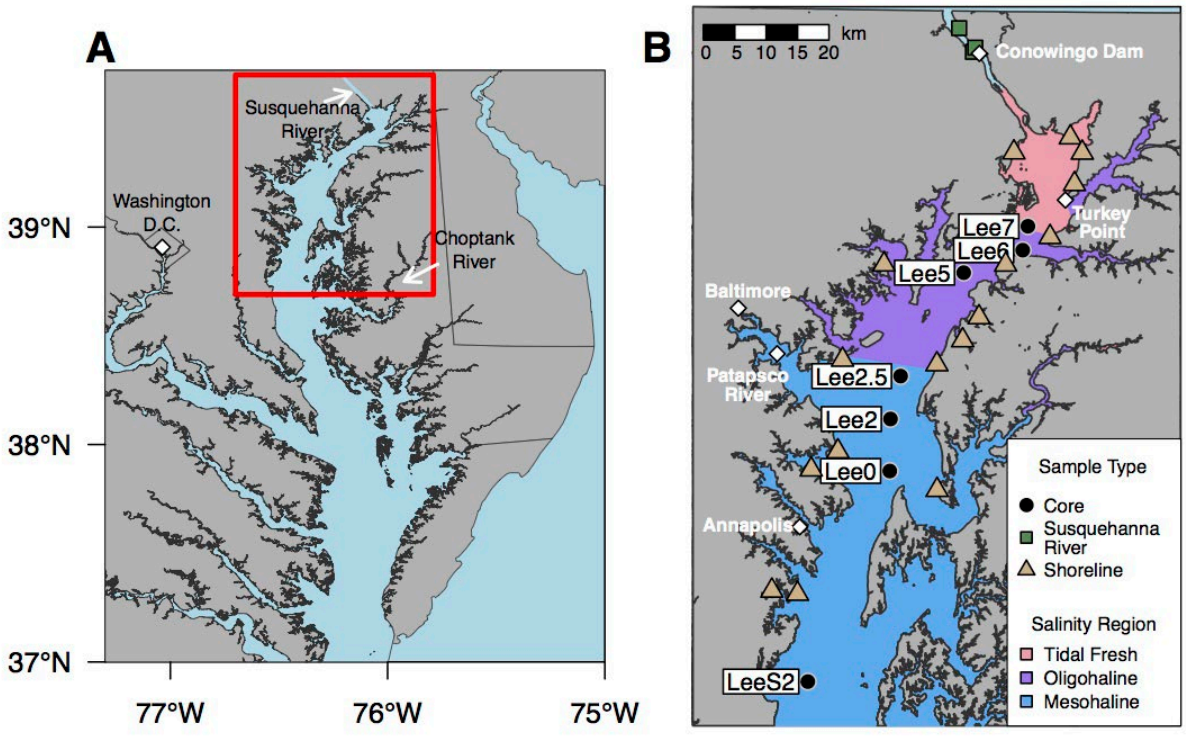

Figure 1. (A) Map of Chesapeake Bay; the red box outlines the area shown in B. (B) Location and names of cores (black circles) and location where Susquehanna River (green squares) and shoreline sediments (tan triangles) were collected. White diamonds indicate the locations of places noted in the text. The major salinity regions are shown in the shading indicated by the legend.

2.2 Field and Laboratory Methods

136 Sediment cores were collected at seven sites in the upper Bay, four of which were
137 sampled with a HAPS box core (http://www.kc-denmark.dk/products/sediment-samplers/haps-
138 corer/haps-core.aspx; 6 cm inner diameter; 30 cm long) on 11 August 2015 (Fig. 1B; Table S1).
139 Box core samples were immediately extruded and sectioned into 1-cm intervals before returning
140 to the laboratory for analysis. All sites were sampled via gravity cores (1.5 m long, 7 cm
141 diameter) on 28 April 2016; revisited sites were within 10 m of sites sampled in August 2015.
142 Intact gravity cores were returned to the laboratory, where they were sectioned into 1-cm (top 20
143 cm) and 2-cm (20 cm-end of core) increments. Sediments from all cores were analyzed for grain
144 size and elemental composition.
145 Field samples were also collected to characterize Susquehanna River and shoreline
146 sediment sources (Fig. 1B; Table S1). Suspended sediment from the Susquehanna River was
147 collected on 6 April 2015 at the Conowingo Dam, the last and largest dam on the Susquehanna
148 River (~15 km upstream of the head of the Chesapeake Bay; Fig. 1B), outlet during high flow
149 (4474 m^3 s^{-1}), using a 20 L carboy. Physical constraints prevented additional water collection at
150 the Conowingo Dam outlet; surface sediments (0-1 cm) from the Conowingo Reservoir with
151 detectable ^{7}Be activity (tracer of recently eroded watershed sediment; Olsen et al. 1986),
152 collected in 2015-2016 (Palinkas and Russ 2019) were assumed to represent Susquehanna River
153 sediment (n=13). Sediment from the three sites closest to the dam was used. Surface grab
154 samples were taken from unprotected, erosive shorelines to represent shoreline sediments (Fig.
155 1B; n=16).
156 Grain size was analyzed by wet-sieving samples at 63 µm to separate the fine (silt+clay;
157 <63 µm) and coarse (sand; >63 µm) fractions. The fine fraction was disaggregated with 0.05%
158 sodium metaphospate in an ultrasonic bath and then analyzed using a Sedigraph 5120. The

coarse fraction was dry-sieved through a standard set of 13 sieves, from 500 µm to 64 µm (at ¼-phi size intervals; phi=-$\log_2$(particle diameter, mm)). The fine and coarse data were joined to calculate median diameters of the bulk sample; median diameters were also calculated for the fine fraction only.

For elemental analysis, two-gram aliquots were taken from the dried surface sediment (0-1 cm) of all box and gravity cores. Seven to nine additional aliquots were taken from dried sediment at ~5-cm increments within gravity cores, for a total of 63 aliquots. Elemental analyses were also performed on Susquehanna River and shoreline sediments. Because element concentrations vary with grain size, such that smaller grain sizes have increased surface area and adsorption efficiency (e.g. Sinex and Helz 1981; Schropp et al. 1991), each aliquot was sieved at 63 µm to minimize variability due to heterogeneous grain sizes; the <63 µm fraction was transferred into a 20-mL plastic scintillation vial. Vials were sent to Bureau Veritas Commodities Canada Ltd. (Vancouver, Canada) for analysis via inductively coupled plasma mass spectroscopy (ICP-MS) to determine concentrations for 59 elements following the methods of Hamilton et al. 2015). For these analyses, 0.25 g sediment split was digested in a 10mL multi-acid solution (2:2:1:1) of H_2O-HF-$HClO_4$-HNO_3 to complete dryness in 50mL Teflon® beakers. The residue was then dissolved in 4mL of 50% HCl and heated to 95°C using a mixing hot block. After cooling to room temperature, the solution was transferred into a 10 mL test-tube and brought to volume using 5% HCl, and analyzed using ELAN® 9000 (https://perkinelmer.com/category/inductively-coupled-plasma-mass-spectrometry-icp-ms-mass). Standard reference materials (NIST 1646a, estuarine sediment; OREAS 25a, ferruginous soil; OREAS 45e, lateritic soil) and replicates were analyzed to determine accuracy and precision,

181 respectively. Elements with >10% uncertainty (19 of the original 59) were omitted from further
182 consideration.
183
184 *2.3 Statistics*
185 All statistical analyses were performed in R version 3.3.2, considering surface
186 (uppermost 1 cm) and core-averaged (>1 cm deep in cores) elemental compositions separately;
187 surface compositions were further divided into spring (April) and summer (August). Core-
188 averaged element concentrations $\overline{(C_e)}$ were calculated using a weighted average approach, based
189 on differing interval thicknesses. For core n,

190 $$\overline{C_e} = \sum_{e,i=1}^{N} C_{e,i} \cdot \frac{h_i}{H} \qquad (1)$$

191 where $C_{e,i}$ is the concentration of element e in interval i, h_i is the thickness of interval i, and H is
192 the total core thickness.
193 Inter-element correlations were quantified using a correlation matrix. Principal
194 component analysis (PCA) was run to reduce the dimensionality of the data and determine which
195 elements explained the most variability across all cores. PCA generates principal components,
196 which are uncorrelated variables made up of linear combinations of the original variables. For
197 each principal component, a loading is assigned to each of the original variables, determined by
198 correlation between the original variable and the principal component. The correlation matrix
199 and PCA were run on all 63 samples (surface and down-core) in order to identify spatial and
200 temporal patterns driving data variability. Simple linear models were developed to compare
201 element concentrations (spring surface, summer surface, and core-averaged values) with distance
202 from the Susquehanna River mouth; p-values <0.05 were considered significant.

Element concentrations were also normalized to those in Susquehanna River surficial sediment. This places all elements on a similar scale and directly compares upper Bay element concentrations to Susquehanna River values without affecting the underlying geochemical patterns. Because silt and clay differences can impact element concentrations, an enrichment factor (EF_{Al}) was calculated that normalizes elemental concentrations to Al (Schropp et al. 1990).

$$EF_{Al} = \left[\frac{Element}{Al}\right]_{sample} / \left[\frac{Element}{Al}\right]_{Susq} \quad (2)$$

In Eq. 2, $[Element/Al]_{sample}$ is the Al-normalized element concentration of the sediment sample, and $[Element/Al]_{Susq}$ is the Al-normalized element concentration of the surficial Susquehanna River sample. The EF_{Al} was only calculated for elements that were correlated with grain size.

A sediment-provenance analysis was then performed, in which source contributions from the Susquehanna River and shoreline erosion were quantified on target (upper Bay) sediments using the United State Geological Survey (USGS) Sediment Source Assessment Tool (Sed_SAT; Gorman-Sanisaca et al. 2017). Differences in element concentrations between Susquehanna River (metamorphic rocks such as schist, gneiss and quartzite, and felsic and mafic igneous intrusions) and shoreline sediment sources (unconsolidated clastic sediments like quartz) were assumed to reflect differences in underlying geology (Markewich et al. 1990). The Sed_SAT tool runs a series of statistical tests to remove outliers, eliminate non-conservative elements, and select a group of elements that best discriminates among different sources. All elements that were correlated with grain size were normalized to Al in both the source and target datasets. Elements that behaved conservatively with a normal distribution were passed into a Forward Stepwise Linear Discriminant Function Analysis (DFA), which selects a combination of elements that best differentiates between the source samples by minimizing the Wilks' lambda

variable (Collins et al. 1997; Gellis and Noe 2013). A Wilks' lambda close to 1 means the sources cannot be distinguished, while a value closer to 0 means the sources are significantly different. A mixing-model analysis using Monte Carlo simulations was then applied, minimizing the following equation:

$$\sum_{i=1}^{n}\{[C_i - (\sum_{i=1}^{m} P_s S_{si})]/C_i\}^2 W_i; with\ \sum_{s=1}^{n} P_s = 1 \quad (2)$$

"where C_i is the concentration of tracer i in the target sample, P_s is the optimized percentage of source type (s); S_{si} is the mean concentration of tracer i in source s; W_i is the weighting factor applied to tracer i; n is the number of tracers in the optimum composite fingerprint; and m is the number of sediment source types" (Gorman-Sanisaca et al. 2017). All elements were included in the first Sed_SAT model run; the second model run excluded elements with non-conservative behavior in the upper Bay.

3. Results

3.1 Correlation Matrix

Individual values of core-averaged bulk grain size, fine-fraction grain size, and element concentrations varied widely in the upper Bay (Table 1). The down-core data were combined with those from spring and summer surficial sediments (Table 2) to calculate a correlation matrix for the 40 elements (Fig. 2). Several of the 40 elements were positively correlated (R^2 values > 0.5) across all study sites (Fig. 2). There were 2 main groups of similarly correlated elements. Group 1 was composed of Li, Mg, Al, K, Sc, V, Cr, Fe, Ga, As, Rb, Tl, and Bi. Most R^2 values for this group were >0.75, but Cr, As, and Bi had lower values of 0.52-0.81. Group 2 was composed of Th, U, and the rare-earth elements (REEs) La, Ce, Pr, Nd, Sm, Eu, Gd, Dy, Y, Er

and Yb. R^2 values in this group ranged from 0.50 to 0.97, with the highest values occurring between the light REEs (La, Ce, Pr, and Nd) and Th.

Table 1. Core-averaged mean (standard deviation) of grain size (first 2 rows) and concentrations of 40 elements at each site. Units in PPM unless specified otherwise in left hand column.

	Lee7 (N=9)	**Lee6** (N=9)	**Lee5** (N=10)	**Lee2.5** (N=9)	**Lee2** (N=10)	**Lee0** (N=8)	**LeeS2** (N=8)
Grain size (μm)	20.75 (7.53)	4.04 (2.04)	2.68 (2.37)	2.72 (1.08)	0.94 (0.44)	0.73 (0.71)	0.60 (0.23)
Grain size <63 (μm)	9.31 (3.49)	3.14 (1.25)	2.26 (1.22)	2.21 (0.69)	0.91 (0.35)	0.67 (0.65)	0.55 (0.28)
Li	42.01 (2.63)	47.57 (5.83)	54.57 (5.74)	66.6 (10.29)	72.09 (5.37)	70.44 (9.92)	82.11 (7.67)
Mg	0.46 (0.03)	0.54 (0.04)	0.61 (0.05)	0.7 (0.09)	0.92 (0.04)	0.89 (0.09)	0.93 (0.04)
Al	4.17 (0.23)	4.72 (0.42)	4.94 (0.39)	5.9 (1.04)	6.88 (0.43)	6.44 (1.09)	7.08 (0.92)
K	1.39 (0.07)	1.56 (0.12)	1.69 (0.08)	1.81 (0.16)	2.27 (0.15)	2.14 (0.28)	2.2 (0.1)
Sc	8.02 (0.55)	8.83 (0.99)	9.4 (0.83)	11.4 (1.85)	12.91 (0.86)	11.93 (2.21)	13.51 (1.96)
V	62.45 (3.26)	74.04 (4.54)	82.5 (7.89)	86.69 (10.84)	105.19 (6.2)	105.43 (14.64)	121.91 (10.43)
Cr	59.77 (8.93)	64.15 (4.75)	67.5 (6.48)	69.67 (6.96)	79.29 (3.89)	74.36 (6.35)	91.56 (6.71)
Fe	2.62 (0.16)	3.07 (0.3)	3.48 (0.45)	3.83 (0.58)	4.35 (0.26)	3.91 (0.73)	4.59 (0.29)
Ga	11.84 (0.94)	13.56 (1.47)	14.46 (1)	15.37 (1.73)	18.53 (1.06)	17.49 (2.43)	19.63 (1.44)
As	6.31 (1.1)	8.98 (0.99)	9.5 (2.69)	14.39 (3.51)	14.19 (1.98)	12.64 (1.23)	20.39 (4.04)
Rb	67.32 (3.15)	75.39 (5.95)	84.55 (5.66)	102.51 (17.3)	117.1 (6.96)	102.89 (20.12)	115.2 (18.21)
Tl	0.46 (0.04)	0.53 (0.06)	0.57 (0.05)	0.61 (0.06)	0.73 (0.05)	0.71 (0.09)	0.77 (0.06)
Bi	0.22 (0.03)	0.29 (0.03)	0.32 (0.07)	0.3 (0.05)	0.43 (0.03)	0.38 (0.06)	0.48 (0.08)
La	35.39 (2.25)	34.81 (1.56)	33.93 (2.02)	38.24 (4.12)	33.3 (2.56)	24.75 (5.26)	32.23 (8.4)
Ce	70.95 (3.26)	71.51 (4.05)	70.87 (4.28)	80.62 (8.79)	70.44 (4.85)	52.19 (11.25)	68.87 (16.91)
Pr	9.11 (0.46)	9.03 (0.44)	9.12 (0.51)	10.09 (1.13)	8.87 (0.5)	6.62 (1.42)	8.68 (2.02)
Nd	34.09 (1.66)	33.8 (1.56)	34.51 (2.09)	40.64 (5.8)	35.01 (2.1)	26.27 (5.5)	33.21 (7.85)
Sm	6.77 (0.38)	6.84 (0.38)	7.2 (0.52)	8.34 (1.36)	6.99 (0.66)	5.6 (1.13)	7.23 (1.55)
Eu	1.29 (0.1)	1.33 (0.11)	1.42 (0.14)	1.58 (0.28)	1.37 (0.12)	1.06 (0.16)	1.38 (0.33)
Gd	5.34 (0.5)	5.89 (0.64)	6.09 (0.59)	6.97 (1.31)	6.16 (0.44)	4.7 (0.63)	6.08 (1.44)
Dy	4.1 (0.3)	4.58 (0.47)	4.79 (0.5)	5.2 (0.9)	4.87 (0.41)	3.73 (0.5)	4.87 (1.03)
Y	19.64 (1.67)	20.55 (1.88)	20.83 (1.65)	23.95 (4.55)	20.97 (1.83)	16.45 (1.75)	21.48 (4.52)
Er	2.12 (0.17)	2.32 (0.13)	2.39 (0.27)	3.01 (0.4)	2.57 (0.21)	2.09 (0.25)	2.73 (0.54)
Yb	2.21 (0.15)	2.35 (0.17)	2.55 (0.25)	2.92 (0.41)	2.47 (0.15)	2.02 (0.17)	2.47 (0.46)
Th	9.8 (0.56)	9.82 (0.41)	10.13 (0.63)	10.24 (0.77)	9.44 (0.51)	7.88 (1.47)	9.97 (2.3)
U	2.97 (0.17)	3.42 (0.29)	3.42 (0.23)	3.91 (0.42)	2.88 (0.22)	2.34 (0.38)	3.65 (0.95)
Na	1.03 (0.08)	1.13 (0.12)	1.19 (0.14)	1.27 (0.16)	2.03 (0.12)	2.65 (0.5)	1.8 (0.75)
P	0.53 (0.16)	0.66 (0.14)	0.75 (0.19)	0.81 (0.21)	1 (0.21)	1.27 (0.39)	0.88 (0.2)
Ca	0.24 (0.04)	0.31 (0.08)	0.22 (0.03)	0.35 (0.15)	0.27 (0.09)	0.26 (0.03)	0.38 (0.25)
Ti	0.32 (0.1)	0.37 (0.03)	0.39 (0.02)	0.35 (0.04)	0.34 (0.01)	0.3 (0.02)	0.34 (0.02)
Mn	934.14 (249.58)	1039.96 (336.96)	1531.27 (319.73)	1348.14 (876.56)	1720.21 (239)	1074.6 (189.24)	695.84 (75.91)
Co	35.18 (7.87)	39.16 (8.04)	39.48 (7.48)	35.3 (16.54)	37.65 (6.01)	34.94 (20.68)	43.08 (8.87)
Ni	52.42 (9.27)	55.03 (8.5)	60.68 (8.82)	52.65 (12.18)	56.86 (6.42)	45.15 (5.08)	55 (6.63)
Cu	124.07 (21.92)	116.55 (31.41)	126.17 (41.19)	142.93 (19.12)	71.99 (45.67)	97.33 (45)	85.63 (12.8)
Zn	185.77 (39.43)	211.65 (45.29)	219.53 (36.14)	200.79 (57.14)	249.2 (12.97)	205.96 (11.34)	304.14 (80.96)
Sr	64.91 (3.94)	78.46 (9.31)	73.62 (4.12)	92 (10.4)	96.24 (5.49)	84.69 (9.49)	95.06 (19.79)
Zr	119.4 (27.08)	125.13 (11.95)	131.74 (12.46)	120.32 (9.58)	93.48 (3.94)	84.82 (10.13)	86.67 (3.14)
Mo	1.45 (0.58)	1.14 (0.54)	1.11 (0.45)	1.54 (0.31)	1.14 (0.22)	1.42 (0.39)	2.25 (0.39)
Ba	337.64	362.08	345.46	350.67	395.64	324.57	234.25

	(23.76)	(42.4)	(14.75)	(39.79)	(19.11)	(65.33)	(58.91)
	46.44	67.23	58.93	67.21		57.06	108.41
Pb	(11.98)	(22.66)	(14.32)	(19.83)	66.91 (4.58)	(17.46)	(24.74)

252

253 Table 2. Surficial spring (top) and summer (bottom) of grain size (first 2 rows) and concentrations of 40 elements at
254 each site. Units in PPM unless otherwise stated

	Lee7	**Lee6**	**Lee5**	**Lee2.5**	**Lee2**	**Lee0**	**LeeS2**
Grain size (µm)	27.23	4.72	3.10	2.08	1.93	2.56	0.97
	21.69		8.13	2.27			1.32
Grain size <63	6.49	3.35	2.99	1.51	1.49	2.34	0.96
(µm)	9.61		3.00	1.78			1.29
Li	38.3	41.5	46.2	46.4	56.7	48.3	75.1
	41.9		43.4	47.8			69.4
Mg (%)	0.5	0.6	0.66	0.57	0.81	0.67	0.91
	0.49		0.57	0.67			0.99
Al (%)	4.21	4.76	4.52	4.11	5.84	4.11	5.46
	4.09		4.37	4.43			5.43
K(%)	1.41	1.7	1.62	1.48	1.91	1.65	2.1
	1.44		1.64	1.76			2
Sc	7.8	8.6	9	8	10.9	7.8	9.7
	7.7		7.7	8.3			9.7
V	64	72	75	68	89	81	113
	61		70	81			96
Cr	55	63	64	57	75	60	86
	47		58	62			78
Fe (%)	2.51	2.88	3.02	2.61	3.64	2.93	4.27
	2.49		2.83	2.99			3.85
Ga	11.79	13.28	13.13	11.67	15.57	12.76	18.07
	10.99		12.82	14.02			16
As	5.5	7.9	8.8	7.6	10.1	10.1	16.2
	6.6		6.7	8.7			11.2
Rb	66	75.9	78.1	73.2	98.9	75.6	94.9
	68.3		78.4	81.3			66.7
Tl	0.43	0.45	0.5	0.44	0.61	0.54	0.69
	0.43		0.47	0.55			0.66
Bi	0.16	0.24	0.35	0.27	0.36	0.53	0.38
	0.16		0.19	0.21			0.31
La	40.4	35.4	34.8	32.4	34.1	25.8	18.2
	37.5		35.7	31.2			13.9
Ce	75.42	71.75	68.96	67.1	69.68	53.74	40.94
	73.63		71.4	64.7			31.12
Pr	9.7	9.2	8.5	8.3	8.4	6.6	5.3
	9.3		9.1	8.1			4.1
Nd	36.4	35.3	33.4	32	34.3	25.4	20.7
	35.5		36.6	30.6			16.1
Sm	6.9	6.5	7	6.5	6	5.1	4.5
	6.6		6.9	5.7			3.7
Eu	1.4	1.4	1.2	1.2	1.3	1	0.8
	1.2		1.3	1			0.8

Gd	5.1	4.5	5.1	4.9	5.2	4.7	3.7
	5.4		5.5	4.8			3.6
Dy	3.6	4	4.1	3.3	4.3	3.1	3.5
	3.4		3.7	4			2.6
Y	18.5	18	19.2	16.7	17.8	14.7	13.9
	17		18	16.5			11.9
Er	2.3	2.3	2.2	2.2	2.5	1.8	1.9
	2		2.2	2.1			1.5
Yb	2.3	2.2	1.9	2.3	2.1	1.9	1.7
	2.2		2.4	2.1			1.5
Th	10.5	9.9	9.5	9	9	7.7	6
	10.6		9.6	8.6			4.6
U	3.1	2.9	3	3	2.7	2.2	2.3
	3.1		3.2	3.2			1.2
Na (%)	0.987	1.048	1.515	1.359	2.134	2.311	2.51
	0.972		1.25	1.506			3.851
P	0.379	0.364	0.464	0.436	0.811	0.729	1.185
	0.375		0.649	0.579			1.123
Ca (%)	0.32	0.38	0.27	0.23	0.25	0.26	0.26
	0.28		0.26	0.23			0.31
Ti (%)	0.459	0.446	0.401	0.379	0.341	0.321	0.329
	0.386		0.358	0.327			0.286
Mn	1048	1438	2014	1987	1538	697	686
	1382		1083	3734			627
Co	22.8	24.1	27.5	23.2	30.1	20.8	25.4
	23.7		22.1	29.5			30.4
Ni	41.5	43.2	46.6	41	46.6	36.2	47
	40.7		39.5	45.9			43.8
Cu	144.2	145	84.7	154.2	210.4	211.7	84
	125		124.8	164			84.4
Zn	142	145	161.7	167	219.4	184.2	254
	131.4		134.6	187.9			215.2
Sr	71	95	84	83	94	76	73
	71		77	81			65
Zr	163.7	142.9	141.2	133.9	97.6	112.4	85.2
	135.7		141.7	117.8			78.7
Mo	0.59	1.09	0.92	1.07	1.03	1.27	1.64
	0.57		0.57	1.13			1.66
Ba	337	393	365	357	368	305	310
	353		353	369			261
Pb	31.74	59.08	50.49	40.97	65.83	103.86	57.77
	32.6		38.83	44.84			65.86

Other correlations between elements with R^2 values > 0.5 were present: Na had a positive correlation with Mg (R^2=0.60) and P (R^2=0.58) and a negative correlation with La, Ce, Pr, Th, and Zr (R^2=0.51-0.58); Zr was negatively correlated with Li, Mg, and Tl (0.50-0.54); Zn was

positively correlated with Cr (R^2=0.63) and Bi (R^2=0.53); and Sr was positively correlated with Al (R^2=0.50) and Rb (R^2=0.52). Correlations between median grain size of the fine fraction and the 40 elements were also evaluated. Although all R^2 values were <0.5 for all elements, group 1 elements tended to have a negative relationship with median grain size (R^2 values 0.37-0.48). R^2 values between median grain size and group 2 elements were < 0.1.

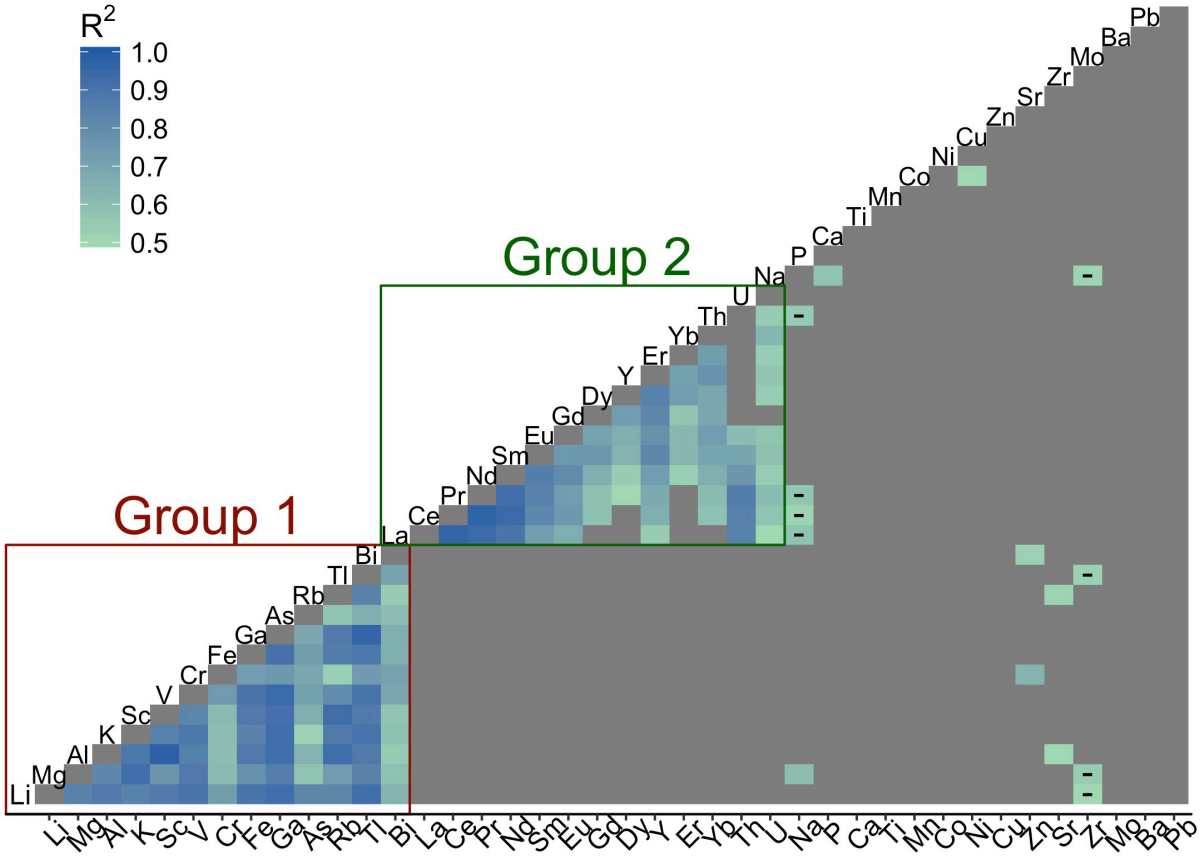

Figure 2. Correlation matrix of 40 elements measured across all upper Bay samples (n=63). To aid in visual interpretation, elements have been organized into groups with similar correlations (red box=group 1; green box= group 2). Black dashes indicate negative correlations (e.g. Na and Zr), and the shading represents the R^2 value for correlations with R^2 >0.5 as noted in the legend (gray indicates R^2<0.5). The x- and y- axes labels correspond to column and row, respectively.

3.2 Element concentrations and enrichment factors

Concentrations of group 1 elements (e.g. Li, Mg, Sc, V, Cr, As, and Bi) in surficial sediments generally increased with distance from the Susquehanna River in both spring and

summer as did core-averaged concentrations (Fig. 3, left column; see Tables 1 and 2 for concentration data). After normalizing to Al, enrichment factors for K, Sc, Ga, Rb, and Tl showed no trend in either spring or summer, with values ~1, while the other elements significantly increased with distance downstream ($p<0.01$; $R^2 = 0.49$-0.98). Core-averaged enrichment factors for K, Sc, Fe, Ga, Rb, and Tl were ~1 and had no relationship with distance downstream. However, enrichment factors for Li, Mg, and As increased downstream ($R^2 = 0.55$, 0.54, 0.74, respectively; Fig. 3, right column). For V and Bi, the core-averaged EF_{Al} increased between Lee7 and Lee5, decreased at Lee2.5, and increased through LeeS2 (Fig. 3, right column); for Cr, the core-averaged EF_{Al} decreased between Lee7 and Lee0, and increased slightly at LeeS2.

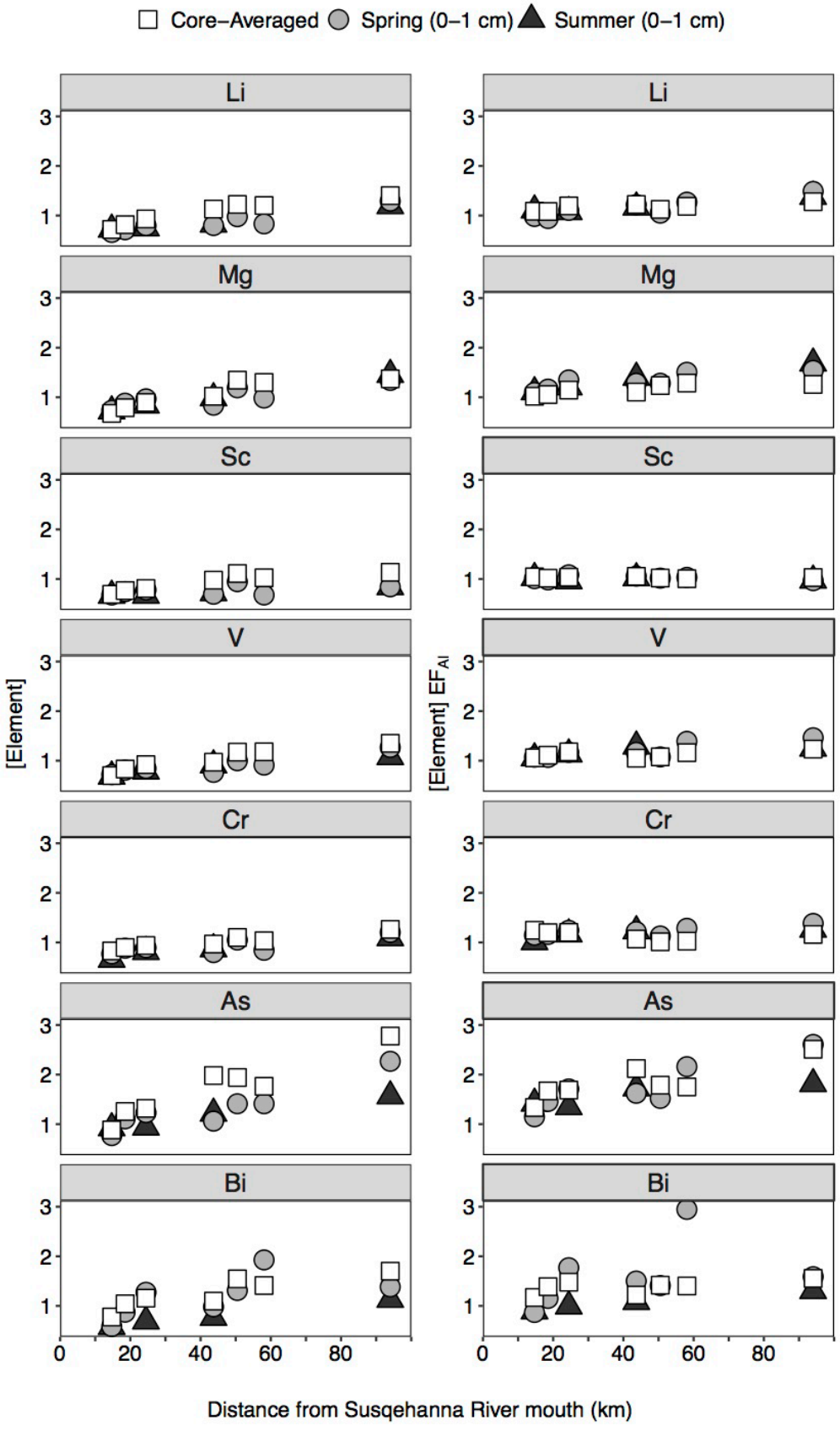
Core–Averaged
Spring (0–1 cm)
Summer (0–1 cm)
Li
Mg
Sc
V
Cr
As
Bi
[Element]
[Element] EF$_{Al}$
Distance from Susqehanna River mouth (km)

284

Figure 3. Examples of observed trends in elements concentrations (Li, Mg, Sc, V, Cr, As, and Bi) with distance from the Susquehanna River mouth. Core-averaged (white squares), spring (0-1 cm) samples (light gray circles), and summer (0-1 cm) samples (dark gray triangles) element concentrations with distance downstream are shown in the left column. Core-averaged, spring, and summer sample enrichment factors (normalized to Al) with distance downstream are shown in the right column. For visual clarity, the element concentrations have been normalized to surficial Susquehanna River sediment concentrations in order to be placed on the same scale.

Because REEs tend to behave similarly over the salinity gradient (Sholkovitz and Szymczak, 2000), total REE concentration was used to assess changes in group 2 elements across study sites (Fig. 4a). Although Th and U were not included, they generally show a similar spatial pattern in both core-averaged and surficial concentrations to the other REEs. Total REE in surface sediments generally decreased with distance downstream, even though there was a slight increase at Lee2 in spring. The core-averaged total REE was relatively uniform between Lee7 and Lee5 (191.01-193.71 ppm), increased to a maximum at Lee2.5 (221.58 ppm), decreased to a minimum at Lee0 (145.45 ppm), and then increased again to 189.24 PPM at LeeS2. REE ratios were also analyzed by comparing the sum of light REEs (LREE; La, Ce, Nd, Pr) to the sum of heavy REEs (HREE; Er, Yb). The LREE and HREE concentrations of each sample were normalized to the LREE and HREE concentrations from Susquehanna River sediment, respectively. There was a slight decrease in surficial (spring and summer) and core-averaged LREE to HREE ratios with distance downstream (Fig. 4b).

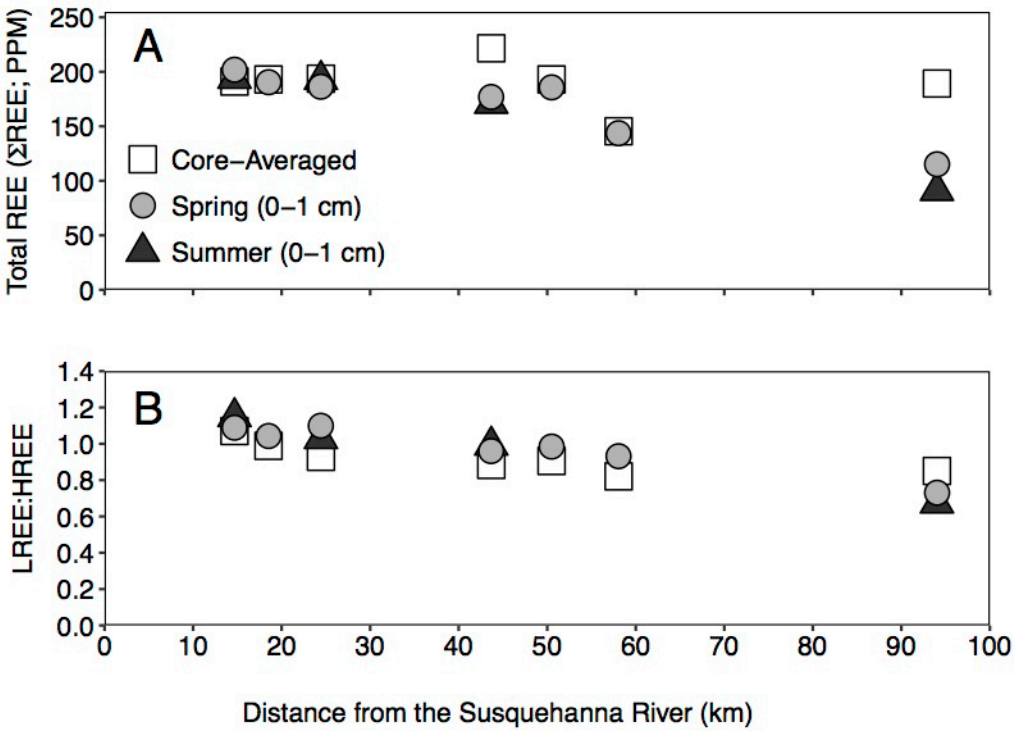

Figure 4. Core-averaged (white squares), spring (0-1 cm) samples (light gray circles), and summer (0-1 cm) samples (dark gray triangles) total REE concentrations (ΣREE) (La, Ce, Pr, Nd, Sm, Eu, Gd, Dy, Y, Er, Yb) in PPM with distance from Susquehanna River sediments (A) and LREE:HREE (ΣLa, Ce, Pr, Nd:ΣEr, Yb (B).

For elements not in groups 1 or 2, spatial patterns of surficial sediments were generally similar in spring and summer (see Table 2). For example, Na and P increased downstream while Zr decreased; surficial Mn increased between Lee7 and Lee2.5 and then decreased at LeeS2. However, surface Mn concentrations at Lee2.5 were nearly two times higher in summer than in spring. The core-averaged concentrations of these elements were more spatially variable (see Table 1): Na and P concentrations increased from Lee7 to Lee0, and decreased at LeeS2; Zr increased from Lee7 and Lee5, and then decreased through Lee0. Mn concentrations increased between Lee7 and Lee2, then decreased through LeeS2.

Core-averaged values were used in the preceding analyses because elemental values did not vary considerably down individual cores. There were some exceptions: group 1 elements As and Bi varied by a factor of 2.5; and group 2 elements varied by up to a factor of 1.5 at Lee0 and

LeeS2. And, distinct concentration peaks were present in the heavy-metal down-core data profiles, particularly for Co, Ni, Cu, Mo, and Pb. For example, peaks in Pb occurred between 30-32 cm at Lee6 (123.07 ppm) and 12-13 cm at Lee2.5 (96.48 ppm); the Pb concentrations then declined towards the surface of the cores (Fig. 5).

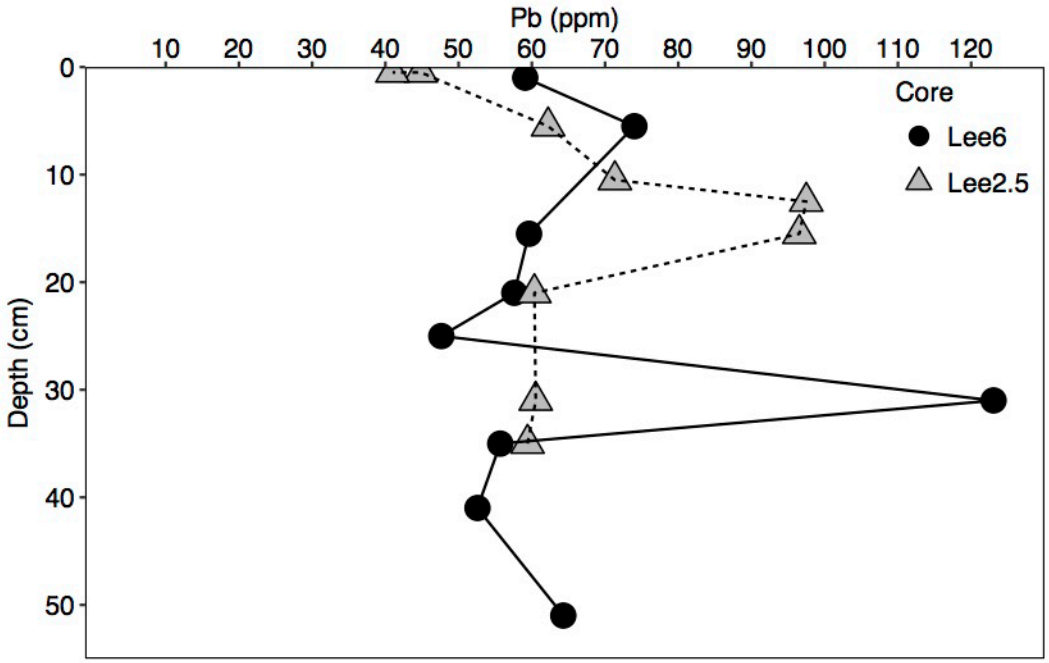

Figure 5. Down-core Pb concentration profile. Black circles and gray triangles represent Lee6 and Lee2.5 profiles, respectively.

3.3 PCA

Principal Component Analysis (PCA) showed that 75.4% of the variability across all samples (surface and down-core) was explained by the first three principal components (38.6%, 29.6%, and 7.2% for PC1, PC2 and PC3, respectively). Elements of group 1 projected strongly onto PC1 (i.e. elements from group 1 had large PC1 loadings relative to PC2), while the elements of group 2 projected strongly onto PC2 (Fig. 6). Grain size also projected strongly onto PC1, but in the opposite direction of the group 1 elements, reflecting negative correlations with these elements. Strontium and Zn projected more strongly onto PC1, while Zr, P and Na had

similar PC1 and PC2 loadings. Calcium, Ti, Mn, Co, Ni, Cu, Mo, Ba and Pb had relatively small loadings in both PC1 and PC2, and therefore did not contribute much to the overall variability on these principal components. Heavy metals Co, Ni, Zn, Mo, and Pb projected strongly onto PC3 (not shown in Fig. 6).

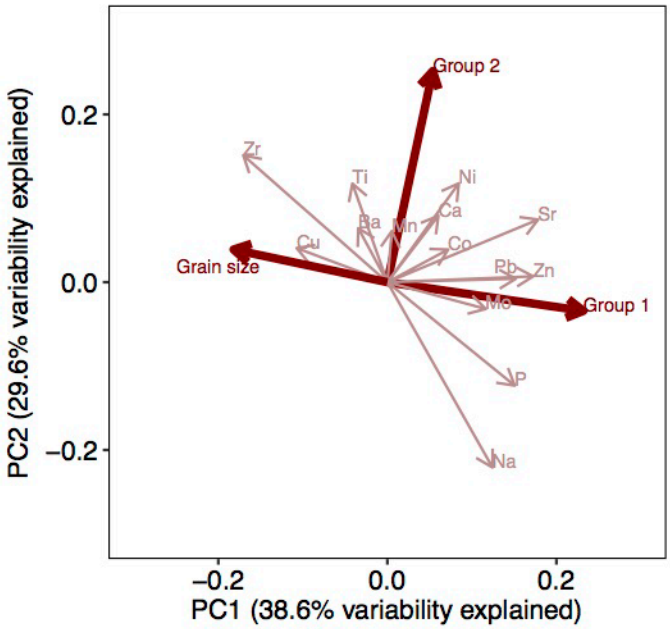

Figure 6. Relative loadings of elements and grain size on the first two principal components. Elements from group 1 and group 2 have been averaged into single vectors (bolded arrows, red text) because of significant overlap among elements in these groups. Vectors for the non-correlated variables (thin arrows, pink text) are also plotted.

Surface (summer 2015 and spring 2016) and core-averaged element concentrations were transformed using the PC1 and PC2 loadings of each element and projected onto the first 2 principal components (Fig. 7). Minimum and maximum PC1 values occurred at Lee7 and LeeS2, respectively, in both summer 2015 and spring 2016 surface sediments. Both spring and summer PC1 values significantly increased with increased distance from the Susquehanna River (p-values 0.03 for both linear regression models), although spring PC1 values at Lee2.5 and Lee0 were outliers. In contrast, summer and spring PC2 values significantly decreased with distance from the Susquehanna River (p-values 0.01 and 0.001 for respective linear regression models).

354 Direct comparisons between spring and summer surficial sediments were possible at Lee7, Lee5,
355 Lee2.5, and LeeS2. In both spring and summer, minimum PC1 values and maximum PC2 values
356 occur at Lee7, and maximum PC1 values and minimum PC2 values occur at LeeS2. However,
357 summer surficial PC1 values were lower at Lee5 than at Lee2.5, but spring values were lower at
358 Lee2.5 than at Lee5. PC2 values were similar between seasons at all sites except LeeS2, where
359 values were lower in summer.

360 Core-averaged PC1 values showed a similar pattern to the surficial sediments, with
361 values generally increasing with distance downstream (p-value=0.003), but over a much larger
362 range. Core-averaged PC1 values at each site were also higher than corresponding surficial PC1
363 values. Core-averaged PC2 values gradually increased from Lee7 and Lee5, reached a maximum
364 at Lee2.5, and then decreased to a minimum at Lee0 (Fig. 7). Core-averaged and surficial PC2
365 values were similar at each site, except at LeeS2, where surficial PC2 values were much lower.
366 Core-averaged PC2 values were significantly higher in the oligohaline (Lee7-Lee2.5) than in the
367 mesohaline (Lee2-LeeS2) regions of the Bay ($p<0.001$). Down-core variability was highest at
368 Lee2.5, Lee0, and LeeS2 and lowest at Lee7, Lee6, Lee5, and Lee2.

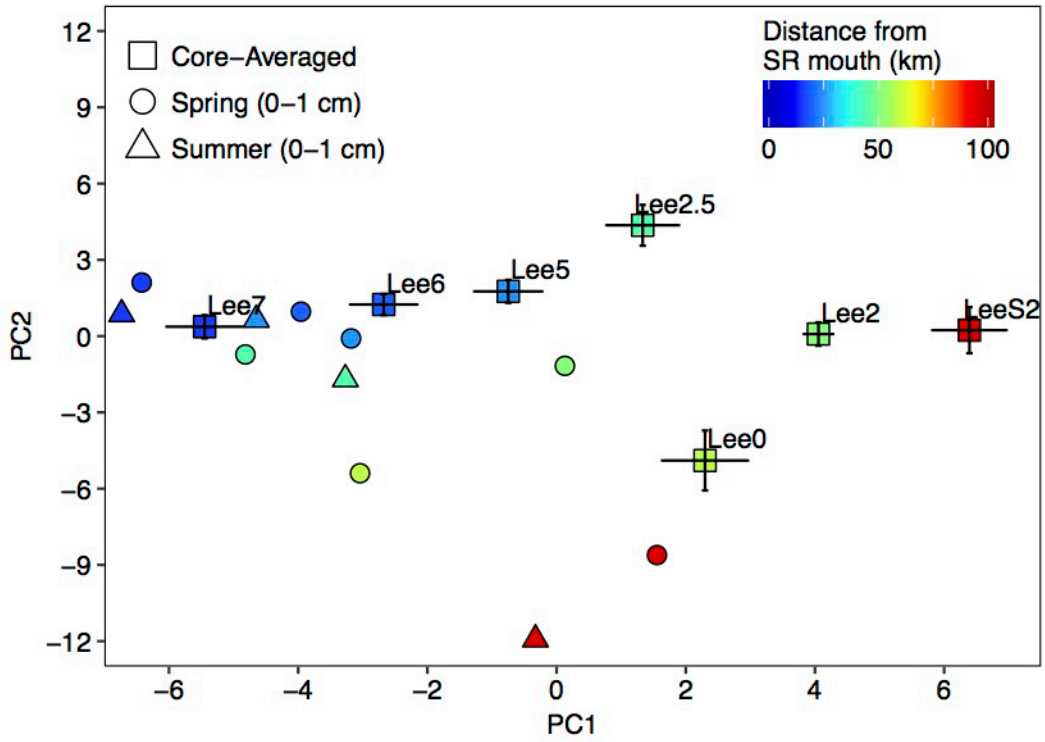

Figure 7. Core averaged (squares), spring (0-1 cm) samples (circles), and summer (0-1 cm) samples (triangles) PC1 and PC2 values across upper Bay sites. Error bars represent standard error of both PC1 (horizontal) and PC2 (vertical) for the core-averaged values.

3.4 Sediment-provenance analysis

Elemental concentrations in shoreline sediments generally varied more widely than concentrations in Susquehanna River sediments (Table 3). The Sed_SAT model was initially run (Run 1) with 38 elements (Na and P were omitted because the concentration results returned were non-numeric; e.g. >10% Na and >5 PPM P) in the source (Susquehanna River and shoreline sediments) and target (upper Bay) geochemical datasets. Only Li, Co, Ti, and Zr behaved non-conservatively in Run 1, and were discarded from further analysis. In Run 1, the group of tracers that best distinguished between sources included As, Tl, Fe, and Ce and correctly classified 96.88% of source sediments; only 1 shoreline site was misclassified as Susquehanna River source. Using this group, sediment-source contributions to upper Bay

384 sediments generally showed Susquehanna influence decreasing with distance downstream, from
385 a core-averaged value of 95.7±0.12% at Lee7 to 75.8±0.90% at LeeS2. Susquehanna sources at
386 Lee2 and Lee0 were outliers from this trend, having comparable values to those at Lee5 (Fig. 8).
387 Down-core percentages did not vary by more than 20%, with the most variability occurring at
388 Lee5, Lee0, and LeeS2.

389 Table 3. Average concentration (standard deviation) of 38 elements at Susquehanna River and shoreline sites.

Element	**Susquehanna River** (N=13)	**Shoreline** (N=16)
Li	55.39 (6.86)	30.7 (10.97)
Mg	0.8 (0.48)	0.71 (0.38)
Al	5.53 (0.76)	3.93 (1.35)
K	2.05 (0.21)	1.5 (0.73)
Sc	9.98 (1.47)	8.72 (3.28)
V	81.31 (12.17)	108.56 (52.22)
Cr	51.92 (10.39)	110.44 (85.19)
Fe	3.39 (0.53)	5.33 (2.55)
Ga	16.27 (2.61)	12.06 (4.07)
As	7.31 (0.96)	23.54 (11.59)
Rb	102.91 (13.96)	63.48 (39.24)
Tl	0.65 (0.1)	0.36 (0.13)
Bi	0.29 (0.06)	0.28 (0.1)
La	37.38 (5.03)	30.59 (10.79)
Ce	78.19 (11.33)	66.48 (24.94)
Pr	8.98 (1.32)	7.58 (2.69)
Nd	37.12 (5.77)	30.09 (10.2)
Sm	7.37 (1.24)	6.16 (2.21)
Eu	1.41 (0.25)	1.26 (0.43)
Gd	6.18 (1.35)	5.32 (1.84)
Dy	4.78 (0.92)	4.38 (1.51)
Y	21.45 (3.83)	20.73 (7.37)
Er	2.52 (0.44)	2.31 (0.84)
Yb	2.48 (0.48)	2.14 (0.79)
Th	9.38 (1.34)	6.94 (2.19)
U	2.72 (0.34)	3.11 (0.91)
Ca	0.88 (2.08)	0.68 (0.45)
Ti	0.21 (0.1)	0.15 (0.07)
Mn	1485.77 (288.64)	2259.5 (1595.43)
Co	33.49 (6.92)	24.65 (16.93)
Ni	57.24 (7.89)	61.89 (38.08)
Cu	95.21 (24.58)	299.94 (184.04)
Zn	207.62 (32.71)	203.33 (95.39)
Sr	106.46 (84.5)	105.12 (27.35)
Zr	69.04 (27.39)	34.29 (34.25)
Mo	0.93 (0.19)	3.02 (1.44)
Ba	475.77 (111.85)	311.19 (140.3)
Pb	38.51 (10.8)	71.88 (64.38)

390

Because the statistical analyses above identified several elements with non-conservative behavior in the upper Bay due to environmental variability (e.g. salinity, oxygen), the second Sed_SAT model run (Run 2) excluded all non-conservative elements. In Run 2, the group of selected elements (Tl and Fe) correctly classified 90% of the source samples, with 3 shoreline sites misclassified as Susquehanna River sites. The Susquehanna River was again the dominant source to upper Bay sediments (Fig. 8), ranging from 89.53±1.57% at Lee5 to 98.32±1.33% at Lee0. Susquehanna River contribution was significantly higher (p-value <0.01) in the Run 2 at all sites except Lee7 and Lee5 (p-value >0.3). The Susquehanna River contribution slightly decreased between Lee7 and Lee5, then slightly increased between Lee5 and Lee0, and again decreased to LeeS2. All cores displayed little down-core variability in Run 2.

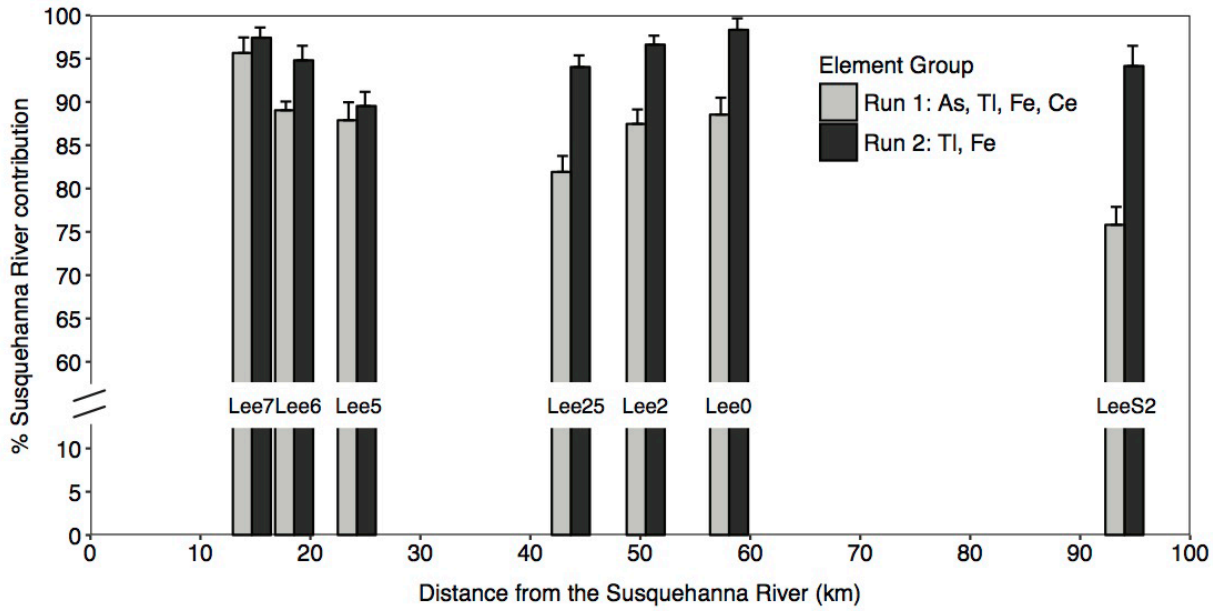

Figure 8. Average percent Susquehanna River source contribution (with error bars) with distance downstream in the first Sed_SAT model run (left; light gray bar) using As, Tl, Fe, and Ce to determine provenance and the second Sed_SAT model run (right; dark gray bar) using Tl and Fe. Note the break in the y-axis scale (between 10 and 60%).

4. Discussion

4.1 Influences on element concentrations in surficial and core-averaged sediments

Correlation matrices and PCA are common techniques for analyzing multivariate sediment geochemistry datasets. They have been applied previously to describe sediment provenance, anthropogenic influence, and changes due to salinity in estuarine sediments (Li et al. 2000; Reid and Spencer 2009; Prajith et al. 2016). Although both techniques are useful for grouping elements with similar patterns, in this study only PCA revealed underlying relationships in the data that explained the most variance.

Elements that are grouped together (i.e. similar R^2 values or PCA loadings) have a common source. For example, in this study, group 1 elements (e.g. Li, Sc, V) accounted for the most variance in PCA. These elements tend to be associated with aluminosilicate clay minerals (Loring 1991; Reid and Spencer 2009), such as illite, chlorite, kaolinite, and montmorillontite. These minerals are prevalent in the Chesapeake Bay (Goldberg et al. 1978), with changing concentrations along the salinity gradient that reflect changes in source (i.e. fluvial or marine) (Feuillet and Fleischer 1980). Although clay mineralogy was not evaluated in this study, the changing concentrations of group 1 elements could be a proxy for changing influence of fluvial versus marine sources; i.e. more fluvial influence near the Susquehanna River. However, while both surface and core-averaged element concentrations increased with distance downstream, these trends are likely driven by differences in grain size, which decreases from silts at Lee7 (most upstream site) to clays at LeeS2 (most downstream site). As grain size decreases, surface area and adsorption efficiency increases (Schropp et al. 1990), resulting in an apparent increase of adsorbed elements. Thus, grain-size effects must be separated from differences in mineralogy through a grain-size correction, such as granulometric or geochemical normalization (Reid and Spencer 2009; Sun et al. 2018). In this study, grain-size influence was removed via enrichment factors (EFs; normalization to Al), which also help discriminate between different sources of

elements, such as terrigenous or anthropogenic sources (Reid and Spencer 2009; Prajith et al. 2016). The EFs were calculated relative to Susquehanna River surficial sediments, so an EF > 1 suggests an additional source of these elements, likely anthropogenic pollution (Sinex and Helz 1981; Prajith et al. 2016). In contrast, an EF ≤1 suggests no or minimal pollution and/or another sediment source with lower concentrations of these elements (Sinex and Helz 1981; Prajith et al. 2016).

While analyzing only the fine fraction of samples minimizes this variability (Sinex and Helz 1981), differences in silt and clay composition can still influence observations. Indeed, the lack of significant trend in the core-averaged EF_{Al} for K, Sc, Ga, Rb, and Tl with distance downstream indicates that differences in silt and clay composition, not differences in sources of these elements, control observed spatial patterns. In contrast, the enrichment of core-averaged EF_{Al} for Mg, As, and Li with increased distance downstream suggests that there is an additional source of these elements. For example, increased Mg can reflect increasing salinity (Elbaz-Poulichet et al. 1984), while increases in As can be due to changing redox condition – under reducing conditions as As can co-precipitate with FeS_2 (Morse and Luther 1999) or become associated with insoluble humic complexes (Guo et al. 1997). Higher As concentrations may also reflect anthropogenic sources (Sanders 1985; Gupta and Karuppiah 1996). Lithium, however, is not typically influenced by anthropogenic sources or biogeochemical processes, but it is highly sensitive to grain-size changes and is sometimes used to correct for grain-size effects (Loring 1991). It is possible that Li concentration changes reflect a shift in dominant sediment source, such as decreasing influence of Susquehanna River sediments and increasing contributions of eroded shoreline sediment (Biggs 1970; Donoghue et al. 1989). Because shoreline sediments have lower Li concentrations than Susquehanna River sediments (Table 3), Li concentrations

should decrease downstream if shoreline sediments become more dominant; however, the opposite trend was observed. The most likely explanation is that grain-size effects were not fully removed when normalizing to Al, and the observed increase in normalized Li concentrations reflects the decreasing grain-size trend (Loring 1991). The non-linear trend of EF_{Al} for V, Cr, and Bi suggest that these elements do not behave conservatively in upper Bay sediments. Changes in surficial and core-averaged V and Cr concentrations could reflect changes in redox conditions, since V tends to precipitate under reducing conditions (Shiller and Mao 1999) and Cr tends to co-precipitate with metal oxides. Changes in Bi concentrations could reflect anthropogenic inputs, since peaks in Bi occur near industrial areas (Baltimore and Annapolis).

Although Na and P were generally not correlated with group 1 elements, they had similar spatial patterns as Mg. The increase in surficial and core-averaged Na with distance downstream could reflect a change in sediment-source contributions and/or the increase in salinity and thus major seawater cations, like Na and Mg (Elbaz-Poulichet et al. 1984). Unlike Na and Mg, P is not a major ion found in seawater but can still vary with changing salinity and redox conditions. A large portion of particulate P is bound to Fe in freshwater but is released at higher salinities and under more reducing conditions (Jordan et al. 2008). This release of P from Fe explains the relatively strong correlation of P and Fe between Lee7 and Lee2 (R^2=0.68) and the lack of relationship at Lee0 and LeeS2. Manganese is also sensitive to redox conditions; high surficial and core-averaged concentrations between Lee5 and Lee2 likely reflect the presence of Mn oxides under oxidizing conditions, and the subsequent decrease between Lee0 and LeeS2 reflects the reduction of Mn to dissolved form under reducing conditions (Guo et al. 1997).

The significant difference between core-averaged PC2 values in the mesohaline and oligohaline reflects the sensitivity of REEs to changes in salinity. At low salinities, REEs are

477 removed from the water column and adsorbed to sediments due to the salt-induced coagulation
478 of riverine colloids (Sholkovitz and Elderfield 1988). As salinity increases, REEs are released
479 from sediments and resupplied to the water column (Sholkovitz and Szymczak 2000). Our results
480 are consistent with these patterns – enrichment of core-averaged REEs at Lee2.5 likely due to
481 salt-induced coagulation of riverine particles, and the subsequent decline at the mesohaline sites
482 suggesting desorption of REEs at higher salinities. Previous work showing a positive linear trend
483 between salinity and water-column REE concentrations implies that there should be a
484 corresponding negative linear trend between salinity and sediment REE concentrations
485 (Sholkovitz and Szymczak 2000). Although core-averaged REE concentrations generally follow
486 this pattern between Lee2.5 and LeeS2, REE concentrations at Lee0 are much lower than
487 expected. REE concentrations are depleted by up to 30% at Lee0, and subsequently increase by
488 ~20% at LeeS2, suggesting either a significant release of REEs from the sediment particles
489 followed by adsorption downstream, or dilution of these sediments by REE-poor sediments
490 (Elderfield et al. 1990; Prajith et al. 2015). Lee0 is located at the mouth of the Chester River,
491 whose watershed is entirely within the Coastal Plain physiographic province. Suspended
492 sediment from the Chester River has REE concentrations that are <10% of the core-averaged
493 REE concentrations measured in Susquehanna River sediments (Table S3), so the low REE
494 concentrations at Lee0 may result from dilution by Chester River sediments and/or shoreline
495 erosion. The decrease in LREE to HREE ratios downstream could either indicate REE
496 fractionation or changes in dominant sediment source. Previous research has shown that HREEs
497 are preferentially released from sediments at mid- to high salinities (Sholkovitz and Szymczak
498 2000), which would increase LREE:HREE in sediment. Therefore, the decreasing trend in our
499 data more likely represents changing sediment sources, supporting the use of REEs for assessing

sediment provenance (Munksgaard et al. 2003) even though they behave non-conservatively. However, average LREE:HREE in Susquehanna River and shoreline source sediments were not significantly different, thus REE ratios were not used for the provenance analyses discussed below.

4.2 Temporal changes in element concentrations

Differences in the spring and summer datasets highlight seasonal shifts in estuarine processes. For example, the differences in PC1 values at Lee5 and Lee2.5 between spring and summer (i.e. PC1 values were lower at Lee2.5 in spring than at Lee5, but were higher at Lee2.5 than at Lee5 in summer) likely reflect seasonal migration of the estuarine turbidity maximum (ETM) (Sanford et al. 2001). In spring, Susquehanna River discharge is high, and the ETM is farther seaward near Lee2.5; in summer, river discharge is lower and the ETM is nearer the head of the Bay and Lee5 (Schubel and Pritchard 1986). In spring, PC1 values of surficial sediments at Lee2.5 are lower than at Lee5, suggesting that fluvial sediment was transported farther downstream (Fig. 7). In summer, surficial PC1 values increase with distance downstream, similar to core-averaged patterns. The only other notable seasonal difference occurs in Mn at Lee2.5. Because this site is near the northern limit of the seasonal anoxic zone (Officer et al. 1984; Gavis and Grant 1986), the high Mn concentrations observed in summer surficial sediments likely represents Mn accumulation at the redox boundary, where dissolved Mn are precipitated as oxides (Burdige 1993).

Differences over longer, decadal time scales are reflected in concentration changes with depth in sediment cores. Generally, there was not much variability with depth in group 1 or 2 elements, which suggests that the sources of these elements and/or estuarine processes impacting

these elements have been consistent over the past ~100 years. However, the slight variability in As and Bi may reflect anthropogenic sources (Gupta and Karuppiah 1996). Heavy metals, included in the third principal component, were the most variable with depth in cores and usually had a distinct peak in the depth profile. These peaks likely represent anthropogenic pollution such as those documented in the Chesapeake Bay (Goldberg et al. 1978; Owens and Cornwell 1995) and other estuaries with significant industrial and population growth throughout the late 19^{th} and 20^{th} centuries (Bricker 1993; Spencer et al. 2003). However, several pollution control measures have been adopted since the late 20^{th} century that reduced heavy metal inputs. These changes are preserved in the sediments; for example, the removal of Pb from gasoline is well documented in previous studies and results in peak concentrations at depths corresponding to the late 1970s in sediment cores (Bricker 1993; Owens and Cornwell 1995; Spencer et al. 2003). These peaks were observed in upper Bay cores, at depth horizons consistent with the late 1970s using accumulation rates from Russ and Palinkas (in revision). Thus, the down-core profiles of heavy metals likely reflect temporal shifts in anthropogenic inputs.

4.3 Sediment-provenance application

We expected to observe decreasing influence of Susquehanna River sediments with distance downstream in the upper Bay, as well as a corresponding increase in shoreline influence. The results from the first Sed_SAT mixing model run (all elements) support this hypothesis. However, the second run of the Sed_SAT mixing model (conservative elements only) indicated unexpectedly high contributions from the Susquehanna River at downstream sites. The differences between the model results using the first (As, Tl, Fe, and Ce) and second

545 (Tl and Fe) groups of elements underscore how sensitive the model is to different groups of
546 elements.

547 The results of the first model run are consistent with previous results based on Fe
548 concentration data (Helz et al. 1985), in which ~85% of bottom sediments in the upper 50 km of
549 the Bay come from the Susquehanna River. Because most of the Susquehanna River sediment is
550 trapped within the ETM (north of Lee2.5) (Donoghue et al. 1989), we expected shoreline erosion
551 to contribute most of the sediments south of Lee2.5. However, Susquehanna River sediment was
552 dominant throughout these cores. It is important to note that the sediment-provenance results in
553 this study represent the source contribution of the fine fraction. And so, one explanation for the
554 relatively high Susquehanna input in our results is that our sites received more fine Susquehanna
555 River sediment than fine shoreline sediment. Susquehanna River source sediments were
556 generally fine (20-30% sand; Palinkas and Russ 2019), but shoreline source sediments were
557 predominately sandy (>90% sand). Indeed, <35% of upper Bay shoreline sediments are
558 composed of fine particles (Schubel 1968) that can be transported into deeper water (Halka
559 2000). Most of the larger, sand-sized shoreline sediments are deposited along shallow shoals
560 immediately adjacent to the shoreline, with relatively little transport beyond nearshore zones.
561 Our results are consistent with these ideas, showing that Susquehanna River sediments contribute
562 more fine sediment in the deeper portions of the upper Bay than shorelines, with increasing
563 contributions from fine shoreline sediments downstream.

564 Although the results from the first model run agree with previous results, the mixing-
565 model analysis included elements with non-conservative behavior in the Bay (As and Ce), as
566 determined by this study. The Sed_SAT tool determines conservative behavior through a range
567 test (i.e. target sediment element concentrations are within the minimum and maximum element

concentrations of source sediments) (Mukundan et al. 2012), without consideration of environmental influence on elemental concentrations. Thus, it is critical to identify environmental influences in a particular study area prior to using Sed_SAT as was done in the second model run. However, the results from this second run were unexpected in that Susquehanna River influence increased downstream, contrasting previous work showing dominance of shoreline sediments in the mesohaline Bay (Biggs 1970). Although the elements selected for the second run behaved conservatively in the upper Bay, these elements did not show any downstream trend after normalizing to Al, which likely explains why source contributions were similar between all sites. A possible explanation for unexpectedly low shoreline-source contributions in this model is the wide variability in Tl and Fe concentrations in shoreline sources (Table 3). The mixing model uses the mean element concentration of each source to quantify its contribution to the target sediments; a wide range in element concentrations results in a mean concentration that may not appropriately represent source sediments. In this case, Fe concentrations (normalized to Al) ranged between 556-680 (average 611) in Susquehanna River sediments and between 545-3114 (average 1453) in shoreline sediments. Target sediment Fe concentrations (normalized to Al), which ranged between 537-782, closer to average Susquehanna River concentration than to average shoreline concentration, resulting in source contributions that indicate greater Susquehanna River influence.

Regardless of the differences between the two model runs, it is clear that the Susquehanna River is the dominant source of fine material near the main channel of the upper Bay, including at downstream sites. While quantifying exact contributions throughout the study area, as well as expected future changes due to natural and anthropogenic activities (climate change, dam infilling) remain fruitful areas for future research, identifying the main source(s) of

591 fine material to the upper Bay is a critical, immediate management need. Sediment-provenance
592 analyses have been applied in freshwater environments to better manage excess sediment inputs
593 (i.e. Walling 2005; Gellis et al. 2009; Devereux et al. 2010; Mukundan et al. 2012); however, it
594 has not, to our knowledge, been applied as a management tool in estuarine environments since
595 one of the main challenges to performing these analyses in estuaries, versus freshwater
596 environments, is that estuarine biogeochemical processes (i.e. changes in salinity, redox
597 condition) alters sediment geochemistry. Excess fine sediment is one of the main pollutants
598 contributing to water quality degradation in the Chesapeake Bay (USEPA 2015), and has been
599 linked to benthic habitat degradation in the Chesapeake Bay, such as oyster reef mortality due to
600 burial (Rothschild et al. 1994; Colden and Lipcius 2016) and loss of submersed aquatic
601 vegetation (SAV) communities as a result of both burial and reduced light availability (Bayley et
602 al. 1978; Dennison et al. 1993). Excess sediments also carry particulate nutrients, which enhance
603 eutrophication by fueling algal blooms that reduce water clarity and lead to oxygen depletion in
604 the water column and/or harmful algal blooms (Kemp et al. 2005). Recent studies have
605 demonstrated that the nutrients associated with sediment particles have more of a deleterious
606 effect on water quality than sediment alone (USACE 2015; Cerco and Noel 2016), and
607 Susquehanna River sediments contain higher nutrient concentrations than shoreline sources
608 (Marcus and Kearney 1991). Sediment-provenance analyses therefore offer a useful tool for
609 quantifying sediment, and by association particulate nutrient, inputs from different sources.
610
611 **5. Summary**
612 This is the first study to report synoptic spatial and downcore geochemical patterns of
613 trace elements, REEs, and heavy metals in bottom sediments of the upper Chesapeake Bay.

614 Statistical analyses on this large dataset reveal element correlations and processes affecting
615 sediment composition. Two groups of elements explain most of the observed geochemical
616 variability: aluminosilicate minerals and REEs reflect grain-size effects and salinity changes,
617 respectively. Heavy metals also influence geochemical variability and were linked to changes in
618 anthropogenic loading. Estuarine sediment provenance was evaluated using conservative
619 elements by comparing geochemical compositions in upper Bay sediments to Susquehanna River
620 and shoreline sediments, and indicated that the Susquehanna River is the dominant source of fine
621 sediment; however, the sediment-provenance tool used to quantify sediment sources utilizes the
622 mean geochemical concentrations, which may misestimate source contributions if source
623 sediments have a large standard deviation. The results of this study indicate that Susquehanna
624 River sediment is a major source of fine sediment near the main channel, both north and south of
625 the ETM. Identifying the main fine sediment source in the upper Bay as well as spatial patterns
626 will help better manage excess sediment inputs and associated nutrients to improve upper Bay
627 water quality.
628
629 **Acknowledgements**
630 We would like to thank Debbie Hinkle, Isabel Sanchez, and Mike Owens for both field
631 and laboratory assistance, as well as Michael Hulme and the crew of the R/V Rachel Carson.
632 Also we would like to thank Ming Li, Karen Prestegaard, and Larry Sanford for their thoughtful
633 feedback on a previous version of this manuscript. This project was funded by a Coastal
634 Resiliency Research Fellowship from Maryland Sea Grant (Russ) under award number
635 NA14OAR4170090 SA75281600-A from the National Oceanic and Atmospheric
636 Administration, U.S. Department of Commerce and Horn Point Laboratory Doughty Fellowship

637 (Russ), and Exelon through the Maryland Department of Natural Resources (Palinkas) for
638 collection and analyses of upper Bay cores. This is UMCES contribution xxxxx.

639 References:

640 Bayley, S., V.D. Stotts, P.F. Springer, and J. Steenis. 1978. Changes in submerged aquatic macrophyte populations
641 at the head of Chesapeake Bay, 1958-1975. *Estuaries* 1: 171. doi:10.2307/1351459.

642 Biggs, R.B. 1970. Sources and distribution of suspended sediment in northern Chesapeake Bay. *Marine Geology* 9:
643 187–201. doi:10.1016/0025-3227(70)90014-9.

644 Blum, M.D., and H.H. Roberts. 2009. Drowning of the Mississippi Delta due to insufficient sediment supply and
645 global sea-level rise. *Nature Geoscience* 2: 488–491. doi:10.1038/ngeo553.

646 Bricker, S.B. 1993. The History of Cu, Pb, and Zn Inputs to Narragansett Bay, Rhode Island as Recorded by Salt-
647 Marsh Sediments. *Estuaries* 16: 589. doi:10.2307/1352797.

648 Burdige, D.J. 1993. The biogeochemistry of manganese and iron reduction in marine sediments. *Earth-Science*
649 *Reviews* 35: 249–284. doi:10.1016/0012-8252(93)90040-E.

650 Cerco, C.F., and M.R. Noel. 2016. Impact of reservoir sediment scour on water quality in a downstream estuary.
651 *Journal of Environment Quality* 45: 894. doi:10.2134/jeq2014.10.0425.

652 Collins, A.L., D.E. Walling, and G.J.L. Leeks. 1997. Source type ascription for fluvial suspended sediment based on
653 a quantitative composite fingerprinting technique. *CATENA* 29: 1–27. doi:10.1016/S0341-8162(96)00064-1.

654 Colden, A.M, and R.N. Lipcius. 2015. Lethal and sublethal effects of sediment burial on the eastern oyster
655 Crassostrea virginica. *Marine Ecology Progress Series* 527: 105–117. doi:10.3354/meps11244.

656 Dennison, W.C., R.J. Orth, K.A. Moore, J.C. Stevenson, V. Carter, S. Kollar, P.W. Bergstrom, and R.A. Batiuk.
657 1993. Assessing water quality with submersed aquatic vegetation. *BioScience* 43: 86–94.
658 doi:10.2307/1311969.

659 Devereux, O.H., K.L. Prestegaard, B.A. Needelman, and A.C. Gellis. 2010. Suspended-sediment sources in an urban
660 watershed, Northeast Branch Anacostia River, Maryland. *Hydrological Processes* 24: 1391–1403.
661 doi:10.1002/hyp.7604.

662 Donoghue, J. F., O.P. Bricker, and C.R. Olsen. 1989. Particle-borne radionuclides as tracers for sediment in the
663 Susquehanna River and Chesapeake Bay. *Estuarine, Coastal and Shelf Science* 29: 341–360.
664 doi:10.1016/0272-7714(89)90033-4.
665 Elbaz-Poulichet, F., P. Holliger, W.W. Huang, and J.M. Martin. 1984. Lead cycling in estuaries, illustrated by the
666 Gironde estuary, France. *Nature* 308: 409–414. doi:10.1038/308409a0.
667 Elderfield, H., R. Upstill-Goddard, and E.R. Sholkovitz. 1990. The rare earth elements in rivers, estuaries, and
668 coastal seas and their significance to the composition of ocean waters. *Geochimica et Cosmochimica Acta* 54:
669 971–991. doi:10.1016/0016-7037(90)90432-K.
670 Feuillet, J.P., and P. Fleischer. 1980. Estuarine circulation; controlling factor of clay mineral distribution in James
671 River estuary, Virginia. *Journal of Sedimentary Research* 50: 267–279.
672 Gavis, J., and V. Grant. 1986. Sulfide, iron, manganese, and phosphate in the deep water of the Chesapeake Bay
673 during anoxia. *Estuarine, Coastal and Shelf Science* 23: 451–463. doi:10.1016/0272-7714(86)90003-X.
674 Gellis, A.C., and G.B. Noe. 2013. Sediment source analysis in the Linganore Creek watershed, Maryland, USA,
675 using the sediment fingerprinting approach: 2008 to 2010. *Journal of Soils and Sediments* 13: 1735–1753.
676 doi:10.1007/s11368-013-0771-6.
677 Gellis, A.C., C.R. Hupp, M.J. Pavich, J. M. Landwehr, W.S.L. Banks, B.E. Hubbard, M.J. Lanland, and J.C. Ritchie.
678 2009. *Sources, transport, and storage of sediment at selected sites in the Chesapeake Bay Watershed*. US
679 Geological Survey Science Investigations Report 2008-5186.
680 Goldberg, E.D., V. Hodge, M. Koide, J. Griffin, E. Gamble, O.P. Bricker, G. Matisoff, G.R. Holdren, and R. Braun.
681 1978. A pollution history of Chesapeake Bay. *Geochimica et Cosmochimica Acta* 42: 1413–1425.
682 doi:10.1016/0016-7037(78)90047-9.
683 Gorman-Sanisaca, L.E., A.C. Gellis, and D.L. Lorenz. 2017. *Determining the sources of fine-grained sediment using*
684 *the Sediment Source Assessment Tool (Sed_SAT)*. U.S. Geological Survey Open-File Report 2017-1062.
685 Guo, T, R.D. DeLaune, and W.H. Patrick Jr. 1997. The influence of sediment redox chemistry on chemically active
686 forms of arsenic, cadmium, chromium, and zinc in estuarine sediment. *Environment International* 23: 305–
687 316. doi:10.1016/S0160-4120(97)00033-0.
688 Gupta, G., and M. Karuppiah. 1996. Heavy metals in sediments of two Chesapeake Bay tributaries — Wicomico
689 and Pocomoke Rivers. *Journal of Hazardous Materials* 50: 15–29. doi:10.1016/0304-3894(96)01773-6.

690 Halka. 2000. *The Impact of Susquehanna Sediments on the Chesapeake Bay*. Chesapeake Bay Program Scientific
691 and Technical Advisory Committee. USEPA Chesapeake Bay Program.
692 Hamilton, P.B., I. Lavoie, S. Alpay, K. Ponader, 2015. Using diatom assemblages and sulfur in sediments to
693 uncover the effects of historical mining on Lake Arnoux (Quebec, Canada): a retrospective of economic
694 benefits vs. environmental debt. *Frontiers in Ecology and Evolution* 3: 99. doi:10.3389/fevo.2015.00099.
695
696 Hannigan, R., E. Dorval, and C. Jones. 2010. The rare earth element chemistry of estuarine surface sediments in the
697 Chesapeake Bay. *Chemical Geology* 272: 20–30. doi:10.1016/j.chemgeo.2010.01.009.
698 Helz, G.R., S.A. Sinex, K.L. Ferri, and M. Nichols. 1985. Processes controlling Fe, Mn and Zn in sediments of
699 northern Chesapeake Bay. *Estuarine, Coastal and Shelf Science* 21: 1–16. doi:10.1016/0272-7714(85)90002-
700 2.
701 Hobbs, C.H., Halka, J.P., Randall T. Kerhin, Michael J. Carron, 1992. Chesapeake Bay Sediment Budget. Journal of
702 Coastal Research 8, 292–300.
703 Jalowska, A.M., B.A. McKee, J.P. Laceby, and A.B. Rodriguez. 2017. Tracing the sources, fate, and recycling of
704 fine sediments across a river-delta interface. *CATENA* 154: 95–106. doi:10.1016/j.catena.2017.02.016.
705 Jordan, T.E., J.C. Cornwell, W.R. Boynton, and J.T. Anderson. 2008. Changes in phosphorus biogeochemistry along
706 an estuarine salinity gradient: The iron conveyer belt. *Limnology and Oceanography* 53: 172–184.
707 doi:10.4319/lo.2008.53.1.0172.
708 Kemp, W.M., W.R. Boynton, J.E. Adolf, D.F. Boesch, W.C. Boicourt, G Brush, J.C. Cornwell, et al. 2005.
709 Eutrophication of Chesapeake Bay: historical trends and ecological interactions. *Marine Ecology Progress*
710 *Series* 303: 1–29. doi:10.3354/meps303001.
711 Kirwan, M.L., and J.P. Megonigal. 2013. Tidal wetland stability in the face of human impacts and sea-level rise.
712 *Nature* 504: 53–60. doi:10.1038/nature12856.
713 Langland, M.J., and T. Cronin. 2003. *A summary report of sediment processes in Chesapeake Bay and watershed*.
714 US Geological Survey Water-Resources Investigations Report 03-4123.
715 Langland, M.J. 2015. *Sediment transport and capacity change in three reservoirs, Lower Susquehanna River Basin,*
716 *Pennsylvania and Maryland 1900-2012*. US Geological Survey Open- File Report 2014-1235.

717 Li, X., O.W.H. Wai, Y.S. Li, B.J. Coles, M.H. Ramsey, and I. Thornton. 2000. Heavy metal distribution in sediment
718 profiles of the Pearl River estuary, South China. *Applied Geochemistry* 15: 567–581. doi:10.1016/S0883-
719 2927(99)00072-4.
720 Loring, D. H. 1991. Normalization of heavy-metal data from estuarine and coastal sediments. *ICES Journal of*
721 *Marine Science* 48: 101–115. doi:10.1093/icesjms/48.1.101.
722 Kerhin, R.T., J.P. Halka, D.V. Wells, E.L. Hennessee, P.J. Blakeslee, N. Zoltan, R.H. Cuthbertson. 1988. The
723 surficial sediments of Chesapeake Bay, Maryland: Physical characteristics and sediment budget. Report of
724 Investigations 48.
725 Marcus, W.A., and M.S. Kearney. 1991. Upland and Coastal Sediment Sources in a Chesapeake Bay Estuary.
726 *Annals of the Association of American Geographers* 81: 408–424. doi:10.1111/j.1467-8306.1991.tb01702.x.
727 Markewich, H.W., M.J. Pavich, and G.R. Buell. 1990. Contrasting soils and landscapes of the Piedmont and Coastal
728 Plain, eastern United States. *Geomorphology* 3: 417–447. doi:10.1016/0169-555X(90)90015-I.
729 Morse, J.W., and G.W. Luther. 1999. Chemical influences on trace metal-sulfide interactions in anoxic sediments.
730 *Geochimica et Cosmochimica Acta* 63: 3373–3378. doi:10.1016/S0016-7037(99)00258-6.
731 Mukundan, R., D.E. Walling, A.C. Gellis, M.C. Slattery, and D.E. Radcliffe. 2012. Sediment Source Fingerprinting:
732 Transforming From a Research Tool to a Management Tool. *JAWRA Journal of the American Water*
733 *Resources Association* 48: 1241–1257. doi:10.1111/j.1752-1688.2012.00685.x.
734 Munksgaard, N.C, K. Lim, and D.L. Parry. 2003. Rare earth elements as provenance indicators in North Australian
735 estuarine and coastal marine sediments. *Estuarine, Coastal and Shelf Science* 57: 399–409.
736 doi:10.1016/S0272-7714(02)00368-2.
737 Officer, C. B., R. B. Biggs, J. L. Taft, L. E. Cronin, M. A. Tyler, and W. R. Boynton. 1984. Chesapeake Bay anoxia:
738 Origin, development, and significance. *Science* 223: 22–27. doi:10.1126/science.223.4631.22.
739 Olsen, C. R., I. L. Larsen, P. D. Lowry, N. H. Cutshall, and M. M. Nichols. 1986. Geochemistry and deposition of ^{7}
740 Be in river-estuarine and coastal waters. *Journal of Geophysical Research* 91: 896.
741 doi:10.1029/JC091iC01p00896.
742 Owens, M., and J.C. Cornwell. 1995. Sedimentary evidence for decreased heavy-metal inputs to the Chesapeake
743 Bay. *Ambio* 24: 24–27.

744 Palinkas, C.M., Russ, E., 2019. Spatial and temporal patterns of sedimentation in an infilling reservoir. *CATENA*
745 180, 120–131. doi:10.1016/j.catena.2019.04.024
746 Prajith, A., Rao, V.P., Kessarkar, P.M., 2015. Controls on the distribution and fractionation of yttrium and rare earth
747 elements in core sediments from the Mandovi estuary, western India. *Continental Shelf Research* 92, 59–71.
748 doi:10.1016/j.csr.2014.11.003
749 Prajith, A., V. P. Rao, and P. Chakraborty. 2016. Distribution, provenance and early diagenesis of major and trace
750 metals in sediment cores from the Mandovi estuary, western India. *Estuarine, Coastal and Shelf Science* 170:
751 173–185. doi:10.1016/j.ecss.2016.01.014.
752 Reid, M.K., and K.L. Spencer. 2009. Use of principal components analysis (PCA) on estuarine sediment datasets:
753 The effect of data pre-treatment. *Environmental Pollution* 157: 2275–2281. doi:10.1016/j.envpol.2009.03.033.
754 Rothschild, B.J., J.S. Ault, P. Goulletquer, and M. Héral. 1994. Decline of the Chesapeake Bay oyster population: a
755 century of habitat destruction and overfishing. *Marine Ecology Progress Series* 111: 29–39.
756 doi:10.3354/meps111029.
757 Sanders, J.G. 1985. Arsenic geochemistry in Chesapeake Bay: Dependence upon anthropogenic inputs and
758 phytoplankton species composition. *Marine Chemistry* 17: 329–340. doi:10.1016/0304-4203(85)90006-4.
759 Sanford, L. P. 1994. Wave-forced resuspension of upper Chesapeake Bay muds. *Estuaries* 17: 148.
760 doi:10.2307/1352564.
761 Sanford, L.P., S.E. Suttles, and J.P. Halka. 2001. Reconsidering the physics of the Chesapeake Bay estuarine
762 turbidity maximum. *Estuaries* 24: 655. doi:10.2307/1352874.
763 Schropp, S. J., F.G. Lewis, H.L. Windom, J.D. Ryan, F.D. Calder, and L.C. Burney. 1990. Interpretation of metal
764 concentrations in estuarine sediments of Florida using Aluminum as a reference element. *Estuaries* 13: 227.
765 doi:10.2307/1351913.
766 Schubel, J.R., and D.W. Pritchard. 1986. Responses of upper Chesapeake Bay to variations in discharge of the
767 Susquehanna River. *Estuaries* 9: 236. doi:10.2307/1352096.
768 Schubel, J.R. 1968. Turbidity maximum of the northern Chesapeake Bay. *Science* 161: 1013–1015.
769 doi:10.1126/science.161.3845.1013.
770 Shiller, A.M., and L. Mao. 1999. Dissolved vanadium on the Louisiana Shelf: effect of oxygen depletion.
771 *Continental Shelf Research* 19: 1007–1020. doi:10.1016/S0278-4343(99)00005-9.

772 Sholkovitz, E. R., and H. Elderfield. 1988. Cycling of dissolved rare earth elements in Chesapeake Bay. *Global*
773 *Biogeochemical Cycles* 2: 157–176. doi:10.1029/GB002i002p00157.
774 Sholkovitz, E., and R. Szymczak. 2000. The estuarine chemistry of rare earth elements: comparison of the Amazon,
775 Fly, Sepik and the Gulf of Papua systems. *Earth and Planetary Science Letters* 179: 299–309.
776 doi:10.1016/S0012-821X(00)00112-6.
777 Sinex, S. A., and G. R. Helz. 1981. Regional geochemistry of trace elements in Chesapeake Bay sediments.
778 *Environmental Geology* 3: 315–323. doi:10.1007/BF02473521.
779 Spencer, K.L., A.B. Cundy, and I.W. Croudace. 2003. Heavy metal distribution and early-diagenesis in salt marsh
780 sediments from the Medway Estuary, Kent, UK. *Estuarine, Coastal and Shelf Science* 57: 43–54.
781 doi:10.1016/S0272-7714(02)00324-4.
782 Sun, X., D. Fan, M. Liu, Y. Tian, Y. Pang, and H. Liao. 2018. Source identification, geochemical normalization and
783 influence factors of heavy metals in Yangtze River Estuary sediment. *Environmental Pollution* 241: 938–949.
784 doi:10.1016/j.envpol.2018.05.050.
785 Thrush, S.F., J.E. Hewitt, V.J. Cummings, J.I. Ellis, C. Hatton, A. Lohrer, and A. Norkko. 2004. Muddy waters:
786 elevating sediment input to coastal and estuarine habitats. *Frontiers in Ecology and the Environment* 2: 299–
787 306. doi:10.1890/1540-9295(2004)002[0299:MWESIT]2.0.CO;2.
788 US Army Corps of Engineers. 2015. *Lower Susquehanna River watershed assessment, Maryland and Pennsylvania*.
789 U.S. Environmental Protection Agency. 2010. Chesapeake Bay Total Maximum Daily Load for Nitrogen,
790 Phosphorus, and Sediment. Retrieved from website: https://www.epa.gov/chesapeake-bay-tmdl/chesapeake-
791 bay-tmdl-document
792 Voli, M,T., K,W. Wegmann, D.R. Bohnenstiehl, E. Leithold, C.L. Osburn, and V. Polyakov. 2013. Fingerprinting
793 the sources of suspended sediment delivery to a large municipal drinking water reservoir: Falls Lake, Neuse
794 River, North Carolina, USA. *Journal of Soils and Sediments* 13: 1692–1707. doi:10.1007/s11368-013-0758-3.
795 Walling, D.E. 2005. Tracing suspended sediment sources in catchments and river systems. *Science of The Total*
796 *Environment* 344: 159–184. doi:10.1016/j.scitotenv.2005.02.011.
797 Windom, H.L., S.J. Schropp, F.D. Calder, J.D. Ryan, R.G. Smith, L.C. Burney, F.G. Lewis, and C.H. Rawlinson.
798 1989. Natural trace metal concentrations in estuarine and coastal marine sediments of the southeastern United
799 States. *Environmental Science & Technology* 23: 314–320. doi:10.1021/es00180a008.

Zimmerman, A.R, and E.A Canuel. 2000. A geochemical record of eutrophication and anoxia in Chesapeake Bay sediments: anthropogenic influence on organic matter composition. *Marine Chemistry* 69: 117–137. doi:10.1016/S0304-4203(99)00100-0.

Zhong, L., and M. Li. 2006. Tidal energy fluxes and dissipation in the Chesapeake Bay. *Continental Shelf Research* 26: 752–770. doi:10.1016/j.csr.2006.02.006.

Table S1. Site coordinates of upper Bay core locations and locations where surficial source sediment was collected from the Susquehanna River and upper Bay shorelines. *Indicates site was reoccupied multiple times.

Site	Coordinates	Date
Upper Bay		
Lee7	39.414°N, 76.079°W*	08/2015
Lee7	39.414°N, 76.079°W*	04/2016
Lee6	39.380°N, 76.088°W	04/2016
Lee5	39.346°N, 76.197°W*	08/2015
Lee5	39.346°N, 76.197°W*	04/2016
Lee2.5	39.197°N, 76.311°W*	08/2015
Lee2.5	39.197°N, 76.311°W*	04/2016
Lee2	39.135°N, 76.328°W	04/2016
Lee0	39.061°N, 76.328°W	04/2016
LeeS2	38.757°N, 76.473°W*	08/2015
LeeS2	38.757°N, 76.473°W*	04/2016
Susquehanna River		
SR1 (Dam)	39.661°N, 76.173°W	04/2015
SR2	39.697°N, 76.211°W*	07/2015
SR3	39.697°N, 76.211°W*	09/2015
SR4	39.697°N, 76.211°W*	12/2015
SR5	39.697°N, 76.211°W*	04/2016
SR6	39.663°N, 76.185°W*	05/2015
SR7	39.663°N, 76.185°W*	07/2015
SR8	39.663°N, 76.185°W*	09/2015
SR9	39.663°N, 76.185°W*	12/2015
SR10	39.663°N, 76.185°W*	04/2016
SR11	39.669°N, 76.181°W*	05/2015
SR12	39.669°N, 76.181°W*	07/2015
SR13	39.669°N, 76.181°W*	04/2016
Shoreline		
Sh1	39.542°N, 76.003°W	04/2017
Sh2	39.520°N, 75.980°W	04/2017
Sh3	39.520°N, 76.107°W	04/2018
Sh4	39.475°N, 75.994°W	03/2018
Sh5	39.399°N, 76.038°W	04/2017
Sh6	39.358°N, 76.120°W	03/2018
Sh7	39.356°N, 76.345°W	04/2018
Sh8	39.283°N, 76.168°W	04/2018
Sh9	39.249°N, 76.197°W	04/2018
Sh10	39.219°N, 76.418°W	04/2018
Sh11	39.214°N, 76.244°W	04/2018
Sh12	39.087°N, 76.424°W	04/2018
Sh13	39.061°N, 76.473°W	04/2018
Sh14	39.034°N, 76.241°W	03/2018

Sh15	38.886°N, 76.541°W	04/2018
Sh16	38.882°N, 76.494°W	04/2018

807

808

Table S2. All element names and chemical symbol described in this manuscript

Element	Symbol
Lithium	Li
Magnesium	Mg
Aluminum	Al
Potassium	K
Scandium	Sc
Vanadium	V
Chromium	Cr
Iron	Fe
Gallium	Ga
Arsenic	As
Rubidium	Rb
Thallium	Tl
Bismuth	Bi
Yttrium	Y
Lanthanum	La
Cerium	Ce
Praseodymium	Pr
Neodymium	Nd
Samarium	Sm
Europium	Eu
Gadolinium	Gd
Dysprosium	Dy
Erbium	Er
Ytterbium	Yb
Thorium	Th
Uranium	U
Calcium	Ca
Sodium	Na
Phosphorus	P
Titanium	Ti
Manganese	Mn
Cobalt	Co
Nickel	Ni
Copper	Cu
Zinc	Zn
Strontium	Sr
Zirconium	Zr
Molybdenum	Mo
Barium	Ba
Lead	Pb

812 Table S3 REE concentrations in Chester River suspended sediments

Element	Concentration (PPM)
La	1.6
Ce	3.31
Pr	0.3
Nd	1.7
Sm	0.5
Eu	<0.1
Gd	0.4
Dy	0.3
Y	1.4
Er	0.2
Yb	0.1

813